






ORIGINAL RESEARCH

# Knockout of Sorbin And SH3 Domain Containing 2 (Sorbs2) in Cardiomyocytes Leads to Dilated Cardiomyopathy in Mice

Jared M. McLendon , PhD; Xiaoming Zhang, MD, PhD; Daniel S. Matasic, MD, PhD; Mohit Kumar, PhD; Olha M. Koval, PhD; Isabella M. Grumbach , MD, PhD; Sakthivel Sadayappan , PhD, MBA; Barry London , MD, PhD; Ryan L. Boudreau , PhD

**BACKGROUND:** Sorbin and SH3 domain containing 2 (Sorbs2) protein is a cytoskeletal adaptor with an emerging role in cardiac biology and disease; yet, its potential relevance to adult-onset cardiomyopathies remains underexplored. Sorbs2 global knockout mice display lethal arrhythmogenic cardiomyopathy; however, the causative mechanisms remain unclear. Herein, we examine Sorbs2 dysregulation in heart failure, characterize novel Sorbs2 cardiomyocyte-specific knockout mice (Sorbs2-cKO), and explore associations between Sorbs2 genetic variations and human cardiovascular disease.

**METHODS AND RESULTS:** Bioinformatic analyses show myocardial Sorbs2 mRNA is consistently upregulated in humans with adult-onset cardiomyopathies and in heart failure models. We generated Sorbs2-cKO mice and report that they develop progressive systolic dysfunction and enlarged cardiac chambers, and they die with congestive heart failure at about 1 year old. After 3 months, Sorbs2-cKO mice begin to show atrial enlargement and P-wave anomalies, without dysregulation of action potential-associated ion channel and gap junction protein expressions. After 6 months, Sorbs2-cKO mice exhibit impaired contractility in dobutamine-treated hearts and skinned myofibers, without dysregulation of contractile protein expressions. From our comprehensive survey of potential mechanisms, we found that within 4 months, Sorbs2-cKO hearts have defective microtubule polymerization and compensatory upregulation of structural cytoskeletal and adapter proteins, suggesting that this early intracellular structural remodeling is responsible for contractile dysfunction. Finally, we identified genetic variants that associate with decreased Sorbs2 expression and human cardiac phenotypes, including conduction abnormalities, atrial enlargement, and dilated cardiomyopathy, consistent with Sorbs2-cKO mice phenotypes.

**CONCLUSIONS:** Our studies show that Sorbs2 is essential for maintaining structural integrity in cardiomyocytes, likely through strengthening the interactions between microtubules and other cytoskeletal proteins at cross-link sites.

**Key Words:** cardiac arrhythmia ■ cytoskeletal dynamics ■ gene expression/regulation ■ heart failure ■ microtubules ■ myocardial contractility

**H**ear failure (HF) remains a leading cause of worldwide morbidity and mortality, attributable in part to multiple causative origins of cardiomyopathy and ineffective treatments. Along with several well-characterized pathogenic molecular signaling

cascades, cardiomyocyte structural and cytoskeletal adapter proteins are known to play a role in HF development and progression. Individual cardiomyocytes string together into myofibers through complex connections that organize intracellular and intercellular

Correspondence to: Ryan L. Boudreau, PhD, Department of Internal Medicine, University of Iowa Carver College of Medicine, 169 Newton Rd, 4334 PBDB, Iowa City, IA 52242. Email: [ryan-boudreau@uiowa.edu](mailto:ryan-boudreau@uiowa.edu)

This article was sent to Céline Fiset, PhD, Guest Editor, for review by expert referees, editorial decision, and final disposition.

Preprint posted on BioRxiv, February 13, 2022. doi: <https://doi.org/10.1101/2022.02.13.480093>.

This work was published in Abstract form in conjunction with Experimental Biology 2020 (FASEB J. 34:1–1. DOI: [10.1096/fasebj.2020.34.s1.07385](https://doi.org/10.1096/fasebj.2020.34.s1.07385)).

Supplemental Material is available at <https://www.ahajournals.org/doi/suppl/10.1161/JAHA.122.025687>

For Sources of Funding and Disclosures, see page 20.

© 2022 The Authors. Published on behalf of the American Heart Association, Inc., by Wiley. This is an open access article under the terms of the [Creative Commons Attribution-NonCommercial-NoDerivs](https://creativecommons.org/licenses/by-nc-nd/4.0/) License, which permits use and distribution in any medium, provided the original work is properly cited, the use is non-commercial and no modifications or adaptations are made.

JAHA is available at: [www.ahajournals.org/journal/jaha](http://www.ahajournals.org/journal/jaha)

## CLINICAL PERSPECTIVE

### What Is New?

- Using available RNA expression data sets, we show that Sorbs2 is consistently dysregulated in human patients and experimental models of ischemic, idiopathic, and hypertrophic cardiomyopathy, and that myocardial Sorbs2 isoforms lack the RNA-binding domain, which has been previously proposed to regulate cardiomyocyte biology.
- In mice with cardiomyocyte-specific deletion of Sorbs2, we find early defects in myocardial microtubule polymerization, left atrial enlargement, and P-wave anomalies, with a subsequent progression toward a dilated cardiomyopathy phenotype, consisting of systolic dysfunction, chamber dilation, and congestive heart failure.
- Using genome- and phenome-wide association data, we identify genetic variants in *SORBS* genes that are associated with cardiovascular-related clinical phenotypes, with notable instances that are consistent with Sorbs2 cardiomyocyte-specific knockout mice phenotypes, including P-wave alterations, left atrial enlargement, and dilated cardiomyopathy.

### What Are the Clinical Implications?

- When integrated with other previous work, these findings show that cardiomyocyte-specific deletion of Sorbs2 is only partially responsible for lethal arrhythmogenic cardiomyopathy observed in global Sorbs2-KO mice, suggesting that other cell types contributing to cardiovascular functions must require Sorbs2.
- This study shows that disruption of Sorbs2 in cardiomyocytes causes early microtubule defects and dilated cardiomyopathy phenotypes, which have been found in other mouse models with altered microtubule-related genes, and future studies should further assess if Sorbs2 mutations are found in patients with cardiomyopathy.
- Beyond the field's focus on the cytoskeletal/sarcomeric proteins themselves, this work highlights and reiterates an important role for cytoskeletal adapter proteins in the onset and development of cardiomyopathy, which could become specific pharmacological and/or genetic screening targets and thus improve the management of heart failure.

cytoskeletons into continuous longitudinal structures via intercalated discs (ICDs) and costameres. ICDs are composed of diverse cell-cell connections, including components of adherens junctions and desmosomes that link actin and desmin networks of adjacent

## Nonstandard Abbreviations and Acronyms

<b>ARVC</b>	arrhythmogenic right ventricular cardiomyopathy
<b>Cx43</b>	connexin 43
<b>DCM</b>	dilated cardiomyopathy
<b>ICD</b>	intercalated disc
<b>NRCM</b>	neonatal rat cardiomyocyte
<b>Sorbs2-cKO</b>	Sorbs2 cardiomyocyte-specific knockout mice
<b>TAC</b>	transverse aortic constriction
<b>WT</b>	wild type
<b>αMHC-Cre</b>	α-myosin heavy chain promoter driving Cre recombinase

cardiomyocytes into cohesive units, as well as gap junctions, which facilitate rapid intercellular electrical conduction and communication through aqueous pores. Costameres attach cardiomyocytes to the extracellular matrix through lateral connections of the sarcomeres to the sarcolemma at z-discs through membrane proteins, cytoplasmic actin, desmin, various actin-associated proteins, integrins, and dystrophin complexes. Disruptions in these structures are found in diseased hearts, showing abnormal conduction and contractile dysfunction. In addition, genome-wide linkage studies for cardiac conduction anomalies and dilated cardiomyopathy (DCM) point to several cytoskeletal structural genes common to the sarcomeres, z-discs, costameres, and ICDs, among others.<sup>1</sup>

Sorbs2 belongs to the *SORBS* family of adaptor proteins that facilitate protein-protein interactions among many cytoskeletal and membrane-associated proteins, including actin, actinin, vinculin, and various signaling kinases. Sorbs2 is relatively broadly expressed across tissues, with highest and enriched expression in cardiac myocytes and smooth muscle-containing tissues.<sup>2,3</sup> Prior reports indicate that Sorbs2 expression is altered in the setting of myocardial infarction and diabetic cardiomyopathy, and its suppression in vitro induces cardiomyocyte hypertrophy.<sup>4–6</sup> In addition, recent in vivo studies suggest both pathogenic and protective roles for Sorbs2 in the development of arrhythmogenic right ventricular cardiomyopathy (ARVC)<sup>7</sup> and left ventricular (LV) noncompaction.<sup>8</sup> Specifically, Ding et al reported that global Sorbs2 knockout mice develop lethal ARVC with severe right ventricular (RV) failure at 4 to 6 months of age. However, Li et al found that Sorbs2 expression increased in LV noncompaction and that adeno-associated virus (AAV)-mediated overexpression of Sorbs2 in mouse hearts caused cardiac hypertrophy and contractile dysfunction within 3 weeks.<sup>8</sup>

Despite clear interest in understanding the relevance of Sorbs2 in cardiac biology and disease, the cell-specific *in vivo* role for Sorbs2 in cardiomyocytes has not been examined using conditional knockout mice. Also, whether myocardial Sorbs2 expression is broadly dysregulated across different cardiomyopathic states in patients and mouse models remains to be systematically evaluated.

Herein, we address these knowledge gaps and report that Sorbs2 expression is consistently upregulated across a variety of cardiomyopathies in humans and rodents, and that cardiomyocyte-specific loss of Sorbs2 in mice is sufficient to cause adverse remodeling of myocardial cytoskeletal proteins. This leads to a progressive DCM phenotype encompassing cardiac conduction defects, systolic and diastolic dysfunction, depressed myofiber contractility, and ultimately congestive HF and premature death, representing an intriguingly distinct phenotype compared with global Sorbs2 knockout mice.<sup>7</sup> While assessing the potential translational relevance of these findings through query of available human genome-wide association study (GWAS) data, we identified several common genetic variants in *SORBS* family genes that are significantly linked to decreased Sorbs2 expression, altered cardiac conduction, and DCM phenotypes that are consistent with our observations in mice.

## METHODS

The data that support the findings of this study are available from the corresponding author on reasonable request.

### Generation of Cardiomyocyte Sorbs2 Knockout Mice

The University of Iowa Animal Care and Use Committee approved all animal experiments described in this article, and procedures were in accordance with institutional guidelines. All rodents used in these studies were housed under 12/12-hour light/dark cycle with access to food and water *ad libitum*. The Sorbs2 floxed mice (Sorbs2 fl/fl), harboring loxP sites flanking Sorbs2 exon 12, were generated by Dr G. Feng<sup>9</sup> and acquired from Jax Labs (stock No. 028600). These mice were intercrossed to C57BL/6J transgenic mice containing the  $\alpha$ -myosin heavy chain promoter-driven Cre recombinase ( $\alpha$ MHC-Cre),<sup>10</sup> provided by Dr. Chad Grueter,<sup>11</sup> to generate Sorbs2 cardiomyocyte-specific knockout mice (Sorbs2-cKO) defined as  $\alpha$ MHC-Cre-positive Sorbs2 fl/fl mice. Most studies used Cre-negative Sorbs2 fl/fl littermates as controls, and some also included transgenic  $\alpha$ MHC-Cre-only mice as additional controls. Both male and female mice were used. Raw

data from physiology experiments were analyzed by investigators blinded to animal genotypes.

### Mouse Models of Cardiac Dysfunction Viruses and Delivery

A cDNA encoding constitutively active calcium/calmodulin-dependent protein kinase II (CaMKII-T287D; gift from Dr. Mark Anderson) was cloned into a standard AAV2-ITR plasmid with a cardiac troponin-T promoter. AAV2/9 viruses were made by the University of Iowa Viral Vector Core. AAV2/9-CaMKII or AAV2/9-green fluorescent protein control viruses were injected into 3-week-old C57/BL6J male mice anesthetized with isoflurane (2%–3%, to effect) via intrajugular vein injection (dose for CaMKII=3.5E+10 viral vector genomes per gram of body weight or green fluorescent protein=1.0E+10 viral vector genomes per gram of body weight), which results in high (>90%) and stable transduction of mouse cardiomyocytes. On the basis of our experience, this CaMKII virus reduces ejection fraction to  $\approx$ 30% within 3 weeks and causes early death by 7 weeks. Herein, mice were euthanized 3 weeks after injection.

### Transverse Aortic Constriction

Minimally invasive transverse aortic constriction (TAC) was performed as previously described with few changes.<sup>12</sup> At the level of the suprasternal notch, a partial sternotomy and thyroid retraction was used to visualize the aortic arch on 8-week-old C57BL/6J male mice anesthetized with ketamine/xylazine (100/10 mg/kg; IP). The aorta was isolated and then constricted with a titanium ligating clip (Teleflex; No. 005200) gapped on 38-gauge acupuncture needles, and placed between the right innominate and left common carotid arteries. Sham mice underwent the same procedure, but without constriction of the aorta. Data shown in [Figure 1C](#) were collected from mice that were euthanized 8 weeks after TAC. Minimally invasive TAC was also performed on wild-type (WT) and Sorbs2-cKO male mice aged 12 weeks. Heart function was evaluated by serial echocardiography, and mice were euthanized after 24 weeks (shown in [Figure 2D–2G](#)).

### Echocardiography

Echocardiography was performed on conscious mice, with mild sedation (midazolam, 5 mg/kg; SC) restrained in the operator's hand, using a Vevo2100 imaging system (VisualSonics, Toronto, ON, Canada). Two-dimensional cine loops were acquired in both long- and short-axis planes to measure standard parameters of cardiac structure and function, according to the endocardial and epicardial area protocol.

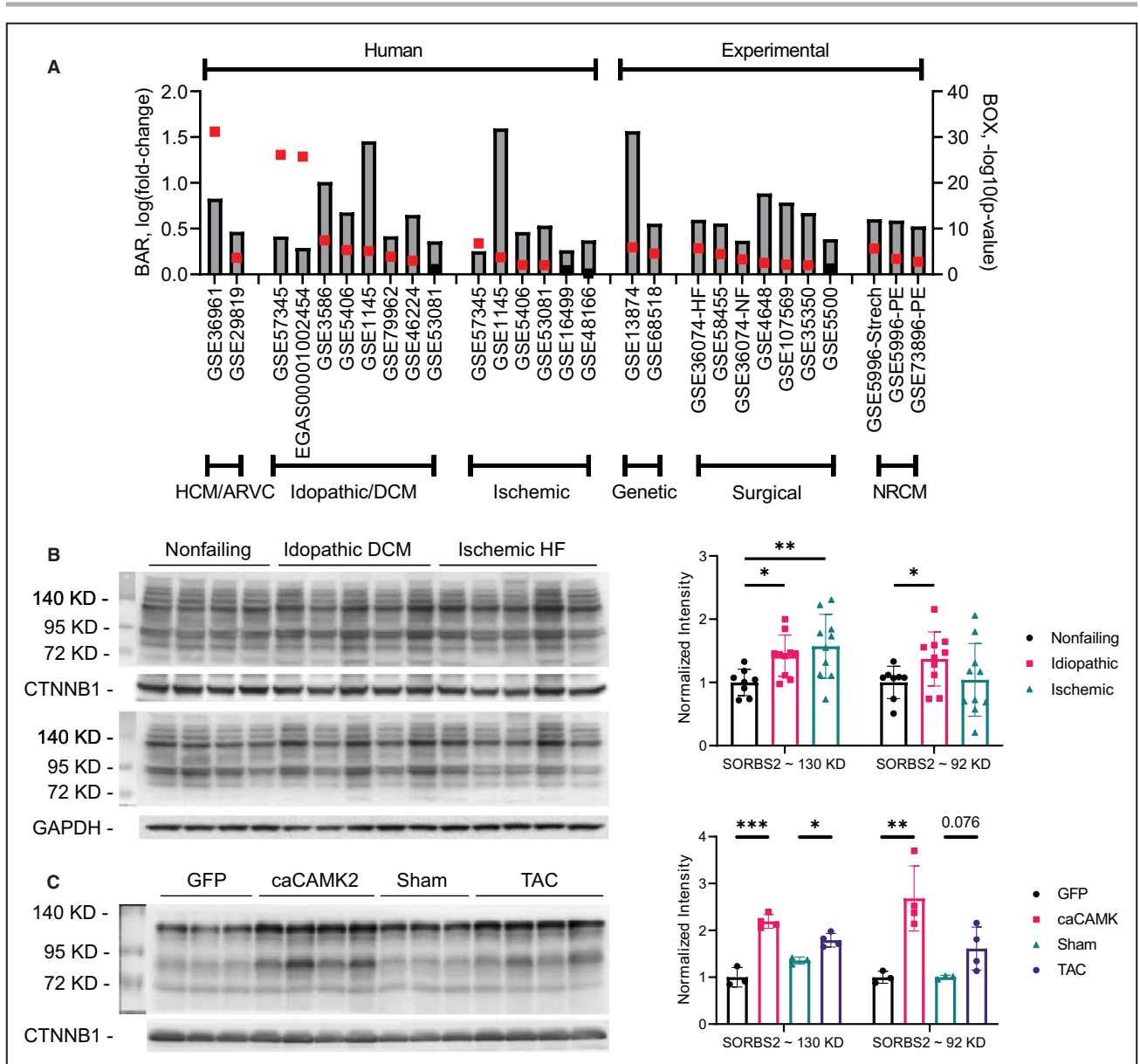


**Figure 1. Sorbs2 is broadly dysregulated in adult cardiomyopathies.**

**A**, Plot showing the log<sub>2</sub> fold change and  $-\log_{10} P$  value for Sorbs2 mRNA expression differences between control samples and cardiac disease and/or experimental samples across the indicated human and rodent transcriptional profiling data sets. Red boxes denote  $P < 0.05$ . Data set accession numbers and relevant group comparisons are noted, and additional information is in Table S2. **B** and **C**, Representative western blot images and quantitative densitometry analysis for expression of major Sorbs2 protein isoforms (130 and 92 kDa) in human heart samples (**B**; N=8–10 per group), or mouse cardiac tissues samples collected from mice treated with control, AAV–green fluorescent protein (GFP), or AAV–caMKII, or subjected to either control sham or transverse aortic constriction (TAC) surgeries (**C**; N=3–4 per group). Data are plotted as mean±SEM. Significance was determined by ANOVA with Dunnett post hoc test, compared with nonfailing controls (**B**) or by 2-tailed *t*-test between control and disease samples (**C**). ARVC indicates arrhythmogenic right ventricular cardiomyopathy; DCM, dilated cardiomyopathy; HCM, hypertrophic cardiomyopathy; HF, heart failure; and NRCM, neonatal rat cardiomyocyte. \* $P < 0.05$ , \*\* $P < 0.01$ , and \*\*\* $P < 0.001$ .

### Electrocardiography

Simultaneous 3-lead ECGs were acquired from anesthetized mice (2% isoflurane) on a heated platform using needle electrodes inserted subcutaneously in limbs (Indus, Rodent Surgical Monitor+ and analog output device). Data were analyzed using standard

mouse settings, including all beats, with time selections of 10 seconds with 4 beat averaging for electrocardiographic analyses, and 60 seconds for heart rate variability analyses (AD Instruments, Powerlab 8/8, Labchart Pro v8.1.13, EKG module v2.4, and heart rate variability module v2.0.3).



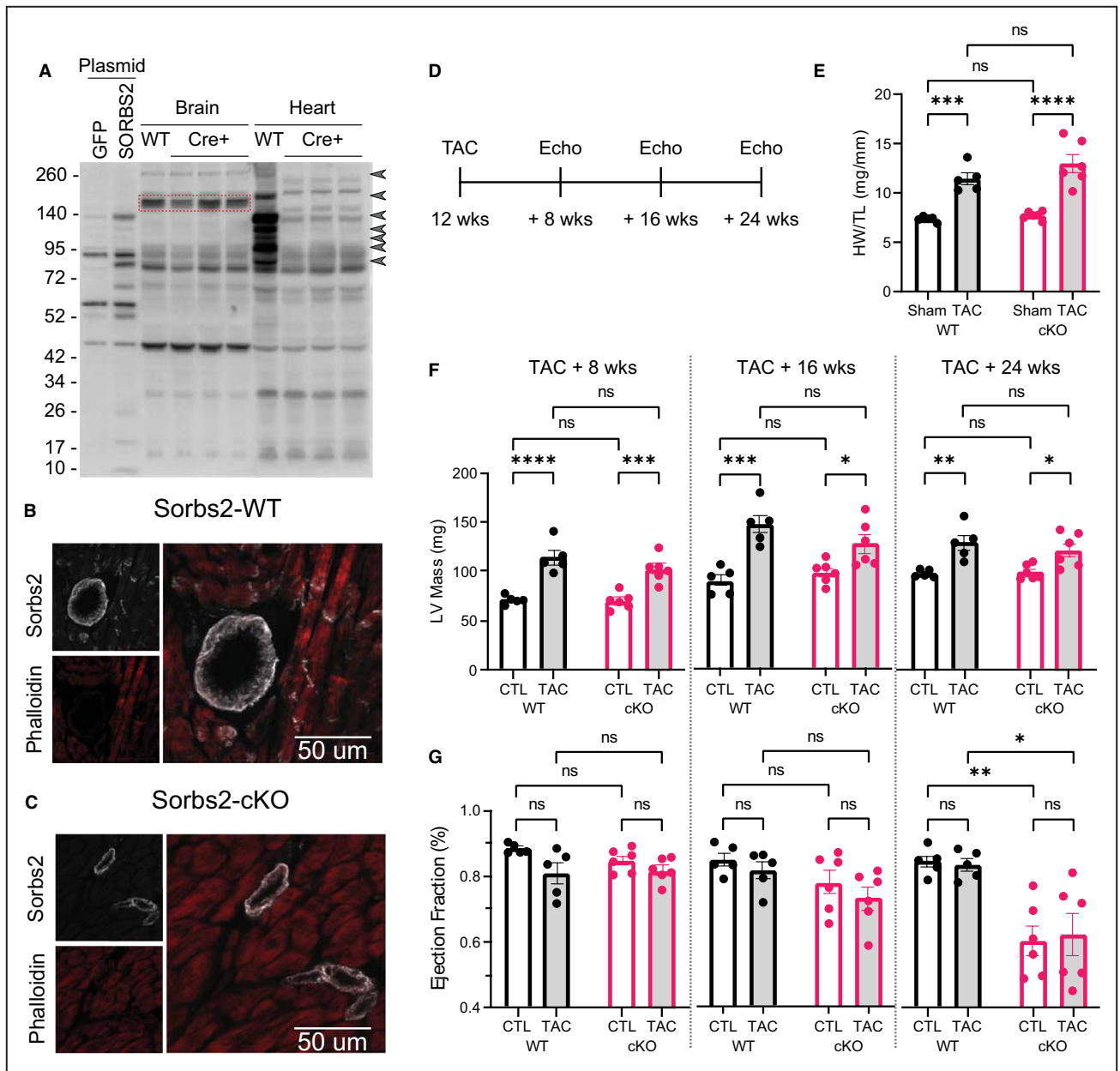


**Figure 2. Generation of novel cardiomyocyte-specific Sorbs2 knockout mice.**

**A**, Sorbs2 western blot in brain and heart tissues from wild-type (WT) and Sorbs2 cardiomyocyte-specific knockout mice (Sorbs2-cKO). The brain-specific Sorbs2 isoform (~150 kDa; red box) remains expressed in WT and CRE+ samples, whereas several immunoreactive bands are lost in CRE+ heart samples compared with control (CTL; arrowheads). The canonical Sorbs2 heart isoform is expected at ~130 kDa. Lysates from cells transiently transfected with expression plasmids encoding either Sorbs2 (mouse cardiac-specific isoform; Figure S2A; “our clone”) or green fluorescent protein (GFP) as control are also included on the blot for reference. **B** and **C**, Representative Sorbs2 immunofluorescence (white) in heart sections from WT and Sorbs2-cKO, costained with phalloidin (red). **B**, In WT hearts, Sorbs2 is prominently expressed in cardiomyocytes at the intercalated disc and in coronary arteries. **C**, In cKO hearts, Sorbs2 is expressed in coronary arteries but not in cardiomyocytes. Tissues are from male mice ~48 weeks old, and scale is 50 μm. **D**, Timeline of transverse aortic constriction (TAC) experiment. **E**, Indexed heart mass (heart weight [HW]/tibia length [TL]) at euthanasia in WT and Sorbs2-cKO mice at ~36 weeks age. **F** and **G**, Left ventricular mass and ejection fraction derived from echocardiography (Echo) at 8, 16, and 24 weeks after TAC. Dots show individual mice (N=5–6/group) with mean±SEM; statistics acquired using 1-way ANOVA with Sidak post hoc test comparing selected groups (each comparison shown on plot). Ns indicates not significant. \*P<0.05, \*\*P<0.01, \*\*\*P<0.001, and \*\*\*\*P<0.0001.

### LV Hemodynamics With Dobutamine Challenge

Mice were anesthetized with 2% isoflurane and placed on a surgical monitoring board to collect ECG and

maintain body heat (Indus, Rodent Surgical Monitor+). Hemodynamics were acquired from a pressure catheter and controller (Millar, SPR-671 and PCU-2000) inserted in the right common carotid artery and pushed

to the left ventricle. For stress tests, a fluid-filled catheter inserted in the left jugular vein was connected to a syringe pump to perform a step-by-step ramped dobutamine infusion maintained for 2 minutes at each step (dose range, 2–12 ng/g per minute).<sup>13</sup> Data were analyzed using standard mouse settings without excluding “outlier” beats and binned into 10-second block averages from baseline throughout the dose response curve (AD Instruments, Powerlab 8/8, Labchart Pro v8.1.13, Blood Pressure module v1.4).

### Myofiber Mechanics

Tissue samples for myofiber mechanics were collected from the left ventricle papillary muscle from flash frozen tissue. Frozen heart tissues were thawed in a calcium concentration 9.0 relaxing buffer (Table S1), trimmed into fiber bundles ( $\approx$ 1 mm long) and skinned overnight in 1% (w/v) Triton X-100. To ensure sarcomeres are properly aligned for mechanical investigations, aluminum T-clips were attached to ends of straight papillary fiber bundles, attached to a force transducer and length controller (Aurora Scientific Inc, Aurora, ON, Canada) and sarcomere length set to 2.1. The fibers were exposed to calcium (dose range, calcium concentration 9.0 to calcium concentration 4.5) obtained by proportional mixing of relaxing and activating buffers (Table S1), as described previously.<sup>14</sup> Fibers were discarded if they exhibited >20% rundown in force over the experiment. Fiber integrity was tested by measuring maximal tension after the experiment (100% activation). Any fibers that did not maintain  $\geq$ 80% maximal tension were excluded from analysis. Muscle dimensions (cross-sectional area and length) were determined using an ocular micrometer and used to normalize contractile force, assuming elliptical fiber shape.

### Western Blot

Frozen heart tissues were homogenized with a bead mill (Qiagen, TissueLyserII) in tissue lysis buffer (Table S1). Homogenates were sonicated, clarified by centrifugation (16 000g, 10 minutes, 4 °C), and normalized by concentration using the bicinchoninic protein assay (Pierce, 23225). Equal masses of protein were separated, transferred, and analyzed using standard western blot techniques with antibodies (Table S1). The loading ranged from 20 to 50  $\mu$ g of total protein per lane, depending on several variables (gel type, size, well format, sample amount, and antibody quality/sensitivity). Most western blots used Biorad Stain-Free gels (item 5678115) with total protein imaged on the gel after running, and membrane after transfer to quantify equal loading and transfer. Others used Nupage 4% to 12% Bis-Tris gels (item NP0336). Images were acquired using enhanced chemiluminescence substrate (Azure, Radiance Plus) on a Biorad Versadoc MP5000 and quantified using

Biorad QuantityOne Software (Version 4.6.6) with global background subtraction settings or acquired using chemiluminescence and/or dual-channel fluorescence on an Invitrogen iBright-1500 and quantified using iBright Analysis Software (Version 4.0.0).

### Microtubule Fraction Assay

Powdered heart tissues (25 mg) were homogenized in 0.25-mL microtubule stabilization buffer (Table S1) with a bead mill (Qiagen, TissueLyserII). Homogenates were centrifuged at 1000g for 5 minutes at 37 °C. The low-speed pellet was reserved, and 0.1 mL of supernatant was centrifuged at 107 000g for 60 minutes at 37 °C. The high-speed supernatant was reserved as the free-tubulin fraction, whereas the high-speed pellet was resuspended in 1% SDS, heated at 90 °C, sonicated to denature proteins, and reserved as the polymerized tubulin fraction. Equal volumes of fractions were analyzed using standard western blot techniques with antibodies (Table S1). Dual-channel fluorescent images were acquired on an Invitrogen iBright-1500 and quantified using iBright Analysis Software (Version 4.0.0).

### Tissue Immunofluorescence

Mouse hearts were sectioned on a coronal plane and frozen in optimal cutting temperature medium. Cryostat sections ( $\approx$ 5  $\mu$ m thick) were affixed to glass slides, postfixed in fresh 4% paraformaldehyde, and permeabilized with 0.2% (v/v) Triton X-100. Slides were blocked, washed, and incubated overnight at room temperature in a humidified chamber with antibodies diluted in blocking buffer (Table S1). After washing, sections were incubated for 90 minutes at room temperature with secondary antibodies diluted in blocking buffer. After washing, slides were mounted with a coverslip using Prolong Diamond (ThermoFisher, P36961) and imaged using a Leica confocal microscope (LSM510) with the  $\times$ 60 oil objective.

### Cell Isolation, Culture, and Transfection

Neonatal rat cardiomyocytes (NRCMs) were isolated from  $\approx$ 3-day-old pups from Sprague-Dawley rats (Charles River, stock 001) following standard protocols using the Worthington Neonatal Cardiomyocyte Isolation System (Worthington, No. LK003300) followed by a 2-step Percoll density gradient,<sup>15</sup> and cultured in cardiomyocyte growth media (Table S1). NRCMs were transfected using Lipofectamine 2000 (0.5% v/v, final) with plasmid DNA (2 ng/ $\mu$ L, final) or siRNA (25 nmol/L; Dharmacon SmartPool) diluted in Optimem media at final volume of 100  $\mu$ L/cm<sup>2</sup>. Sorbs2 expression plasmid was generated by reverse transcriptase–polymerase chain reaction amplification of a mouse cardiac-specific Sorbs2 isoform (primers listed in Table S1) and subsequent cloning into a

cytomegalovirus expression vector. The transfected cells were incubated for 4 hours before transfection medium was removed and replaced with growth medium. The cells were incubated for  $\approx$ 48 hours with daily medium exchanges before patch-clamp electrophysiology or calcium imaging experiments.

### Determination of Cytosolic $\text{Ca}^{2+}$ Transients

NRCMs were loaded with Fura-2 acetoxymethyl ester by incubating cells with 1  $\mu\text{mol/L}$  Fura-2 acetoxymethyl ester in Hanks balanced salt solution for 20 minutes at room temperature and incubated at 37  $^{\circ}\text{C}$  for 20 minutes to esterify the stain. Cells were excited alternatively at 340 and 380 nm. Fluorescence signal intensity was acquired at 510 nm. Real-time shifts in Fura-2 acetoxymethyl ester fluorescence ratio were recorded about 30 seconds before adding an agonist using a Nikon Eclipse Ti2 inverted light microscope. Imaging was acquired every 2 seconds to measurement. Peak amplitude was calculated by subtracting the baseline fluorescence ratio from the highest fluorescence ratio. The area under the curve was determined using GraphPad Prism and normalized by subtracting the area under the curve at baseline. Summary data represent the average difference in the basal and peak increase in cytoplasmic  $[\text{Ca}^{2+}]$ .

### Whole-Cell-Patch Clamp of $\text{Na}^+$ Currents

All whole-cell recordings were obtained using the Axon Axopatch 200B amplifier and Digidata 1440B data acquisition system (Molecular Devices), as previously described.<sup>16</sup> Cell capacitance was recorded after adjusting for transients postmembrane rupture. pClamp software (version 10.4) was used for data analysis. To calculate sodium current density, peak current was divided by the membrane capacitance. To test steady-state activation of sodium current in NRCMs, a 200-ms prepulse to  $-120$  mV was used to eliminate inactivated channels, and cells were subjected to a 200-ms test pulse between  $-80$  and  $15$  mV in increments of 5 mV. Patch pipettes of 2 to 3  $\text{M}\Omega$  were used, and recipes for internal and extracellular solutions are listed in (Table S1).

### Bioinformatics

Data were exported for additional analyses using Microsoft Excel, Graphpad Prism v8.2.1, and R v3.6.1. RNA-sequencing and ribosomal-sequencing data were acquired from <http://shiny.mdc-berlin.de/cardiac-translatome/>,<sup>17</sup> or remapped from sequence read archive entries PRJNA477855<sup>18</sup> or PRJNA484227.<sup>19</sup> Relevant data sets of RNA expression were pulled from Gene Expression Omnibus, the European Genome-Phenome Archive, or published supplementary data

tables. Select data were reanalyzed using GEO2R webtool comparing the difference between cardiomyopathy versus control samples (data sets described in Table S2). GWAS data (Table) were acquired from these publications/databases.<sup>3,20–28</sup>

### Human Cardiac Tissue Samples

LV cardiac tissues were obtained from the University of Pennsylvania Human Heart Bank (Dr. Kenneth Margulies). All subjects donating tissue provided consent under an approved institutional review board protocol, with relevant clinical information confidentially linked to the specimens in deidentified manner. LV free-wall tissue was harvested at the time of transplantation surgery from subjects with heart failure or from unused nonfailing donor hearts. Hearts were perfused with cold cardioplegia before cardiectomy to halt contraction and prevent ischemic damage.

### Statistical Analysis

Data were analyzed for statistical significance using various analyses in Microsoft Excel, Graphpad Prism v8.2.1, and R v3.6.1. Generally, individual replicates are plotted with mean $\pm$ SEM, and statistical significance is directly stated or indicated by convention ( $*P<0.05$ ,  $**P<0.01$ ,  $***P<0.001$ ,  $****P<0.0001$ , ns=not significant). Descriptions of specific tests are included in accompanying figure legends. Pairwise comparisons were made using 2-tailed *t*-tests. Comparisons among  $>3$  groups used 1-way ANOVA with the indicated post hoc tests comparing selected groups (each comparison is shown on graphs). Survival was compared using a log-rank test (Mantel-Cox method). Trendlines on continuous data are fit with a locally weighted smoothing nonlinear regression model. In addition, continuous data are binned into appropriate blocks and analyzed using a repeated-measures 2-way ANOVA with Sidak multiple comparisons testing the interaction between age and genotype. Trendline on myofiber mechanics denotes a least-squares fit to sigmoidal dose-response curve with variable slope.

## RESULTS

### Sorbs2 Is Broadly Dysregulated in Cardiomyopathic Hearts

Previous reports indicate that Sorbs2 expression is increased in heart samples from patients with LV noncompaction<sup>8</sup> and in serum following myocardial infarction,<sup>4</sup> and genetic mutations in Sorbs2 may underlie ARVC.<sup>7</sup> However, there are no published efforts interrogating the broad dysregulation of Sorbs2 mRNA expression in diseased hearts. In a systematic analysis of several independent data sets of transcriptome-wide

RNA expression, accessed from public data repositories, we examined Sorbs2 expression in nonfailing and diseased hearts from human subjects and rodent models. In 13 of 16 data sets from independent human cohort studies, Sorbs2 mRNA expression is significantly increased in patients with ischemic, idiopathic, ARVC, and hypertrophic cardiomyopathy (Figure 1A). In-depth analysis of an available RNA-sequencing data set<sup>18</sup> revealed that the most abundant cardiac Sorbs2 transcript isoforms are among those significantly increased in dilated and ischemic cardiomyopathy (Figure S1A through S1C). Interestingly, this increase is conserved across species, as Sorbs2 mRNA levels are also consistently higher in 12 of 13 data sets from experimental rodent models of cardiac hypertrophy, ischemia, or genetic cardiomyopathies (Figure 1A).

To assess if Sorbs2 expression is also elevated at the protein level, we performed western blot analyses and found that Sorbs2 protein expression is increased  $\approx 50\%$  in human cardiac tissues from patients with ischemic or idiopathic HF, compared with nonfailing control samples (Figure 1B, demographics in Table S3). In mice, Sorbs2 protein expression was also increased  $\approx 2$ -fold in failing hearts induced by cardiac-targeted overexpression of constitutively active CaMKII, which elicits severe HF (ie, reduced ejection fraction [EF] down to  $\approx 20\%$ – $30\%$ ) within 3 weeks (time of collection) and early death by 7 weeks. In addition, Sorbs2 protein levels were increased by  $\approx 50\%$  in mouse hearts subjected to mild pressure overload, resulting in cardiac hypertrophy and cardiac dysfunction (ie, 40%–50% increase in heart weight/body weight ratio and  $\approx 10\%$ – $15\%$  decrease in EF) by 8 weeks (Figure 1C, phenotyping data in Table S4).

To assess if Sorbs2 upregulation in HF occurs through transcriptional or posttranscriptional mechanisms, we queried ribosomal profiling (ribosomal-sequencing) data from human failing hearts.<sup>17</sup> Normalized RNA-sequencing and ribosomal-sequencing reads were significantly upregulated in nonfailing and DCM samples and calculated translational efficiency (ribosomal/RNA ratio) was equal to one independent of disease (Figure S1D). This suggests that cardiac Sorbs2 transcripts are not likely under substantial translational regulation at baseline or during HF. Altogether, these expression analyses indicate that independent of the causative origin, myocardial Sorbs2 expression is broadly and consistently increased in the setting of HF, in both human patients and rodent models, likely through transcriptional upregulation or increased transcript stability.

### Examination of Sorbs2 Cardiac Isoforms

Sorbs2 is a large gene with complex splicing that gives rise to numerous transcripts (eg, the Ensembl

human genome assembly currently annotates 65 transcripts, including 8 with complete coding sequence) (Figure S1A through S1C). To assess the gene structure of Sorbs2-encoding cardiac mRNA isoforms, we reanalyzed available RNA-sequencing and ribosomal-sequencing data from human and rodent heart tissues<sup>17,19</sup> to determine which exons are expressed at the RNA level and translated into protein, focusing on the 8 isoforms harboring complete coding sequence (Figure S2A). Assessment of protein domains across Sorbs2 shows that the characterized cytoskeletal adaptor domains (sorbin homology and SRC Homology 3, SH3) are present in each isoform, including those expressed in heart; however, of note, the characterized RNA-binding domain (ZnF-C2H2) is restricted to select transcripts that are not present in cardiac tissue. Along these lines, we examined sequences of Sorbs2 transgenes described in published studies related to cardiomyocyte biology and note that the transgene (Addgene No. 74514) used to demonstrate RNA-binding activity in cardiomyocytes<sup>29</sup> does not represent a Sorbs2 isoform expressed in cardiomyocytes. The exon harboring the RNA-binding domain is exclusively expressed in neuronal tissues, and this transgene was originally cloned from mouse brain. Although it is clear that much more work is needed to better understand the complexity of Sorbs2 isoforms and their relevance to cardiac biology, this analysis reveals that the cytoskeletal adaptor domains are present in every cardiac isoform, whereas the RNA-binding domain is not expressed in heart.

### Generation of Cardiomyocyte-Specific Sorbs2 Knockout Mice

Sorbs2 is consistently upregulated in failing hearts, and Li et al recently found that AAV-mediated Sorbs2 overexpression in mouse heart causes HF within 3 weeks.<sup>8</sup> Loss of Sorbs2 has also been connected to cardiomyopathy phenotypes in humans and mice<sup>7,29</sup>; however, the cell-specific role for Sorbs2 in cardiomyocytes has not been examined using conditional knockout strategy. Sorbs2 is broadly expressed in many tissues, with highest expression in cardiac myocyte- and smooth muscle-containing tissues. To dissect the role of Sorbs2 specifically in cardiomyocytes, we created Sorbs2-cKO by interbreeding  $\alpha$ MHC-Cre transgenic mice with Sorbs2 fl/fl mice (loxP sites flanking Sorbs2 exon 12) (Figure S2B, red box). Excision of this obligate exon, present in all Sorbs2 protein-coding transcripts expressed in mouse hearts (transcripts per million  $>1$ ), will introduce a frameshift and premature termination. Sorbs2-cKO mice are viable and fertile and have a normal development and maturation. Western blot analysis of tissue lysates confirmed the loss of Sorbs2 protein expression in Sorbs2-cKO heart samples, relative to



WT controls (Sorbs2 fl/fl, Cre-negative mice), whereas Sorbs2 protein expression persisted in Sorbs2-cKO brains (Figure 2A). Notably, cardiomyocyte loss of Sorbs2 does not lead to a compensatory upregulation of Sorbs1 in heart tissues (Figure S3A and S3B). Conditional Sorbs2 deletion was also examined by immunofluorescent staining of cardiac tissue sections, which showed cardiomyocyte-specific loss of Sorbs2 protein in Sorbs2-cKO mice, evidenced by overt lack of Sorbs2-positive staining at the ICD and retained expression in coronary artery smooth muscle (Figure 2B and 2C and Figure S3C). Together, these data support the successful generation of cardiomyocyte-specific Sorbs2 knockout mice, with retained expression in other tissues and cardiac cell types.

### Sorbs2 Expression in Cardiomyocytes Is Not Required for Cardiac Hypertrophy

Sorbs2 is consistently upregulated in HF and cardiac hypertrophy. AAV-mediated Sorbs2 overexpression induced cardiac hypertrophy in mice<sup>8</sup>; however, whether Sorbs2 is required for compensatory cardiac hypertrophy has not been addressed. We tested the hypothesis that Sorbs2-cKO mice subjected to pressure overload will generate insufficient compensatory hypertrophy and have rapid and severe heart failure. Male WT and Sorbs2-cKO mice were subjected to cardiac pressure overload by TAC at 12 weeks of age (Figure 2D). Serial echocardiography measures (collected at 8, 16, and 24 weeks after TAC) and gravimetric analyses done at the time of euthanasia (24 weeks after TAC) showed significant increases in heart size (heart weight normalized to tibia length) and LV mass in both WT and Sorbs2-cKO mice after TAC, relative to sham surgery controls; however, no genotypic differences were found (Figure 2E and 2F). Further assessment of echocardiography data to assess cardiac function revealed that, compared with WT mice, both sham control and TAC Sorbs2-cKO mice have significantly decreased EF by 24 weeks after TAC (ie, 36 weeks of age) (Figure 2G). Together, these data suggest that cardiomyocyte Sorbs2 is not required for cardiac hypertrophy and that Sorbs2-cKO mice develop progressive HF independent of pressure overload.

### Cardiomyocyte-Specific Sorbs2 Knockout Mice Develop Age-Related Systolic Dysfunction, Cardiac Remodeling, and Premature Death

To better understand when loss of cardiomyocyte Sorbs2 impairs cardiac function in mice, we performed serial echocardiography in WT (fl/fl-CRE negative), Sorbs2-cKO, and  $\alpha$ MHC-Cre only mice from about 10 weeks through 16 months of age (representative M-mode shown in Figure S4A). Compared with controls,

Sorbs2-cKO hearts show a progressive DCM phenotype characterized by reduced LV EF (Figure 3A), increased LV chamber dilation (Figure 3B), and thinned LV wall thickness (Figure 3C), with significant differences first appearing after 30 weeks in EF, 40 weeks in dilation, and 50 weeks in wall thickness (Figure 3A through 3C plots continuous data, and summary statistics of binned data and analyses are presented in Table S5). Left atrial (LA) enlargement becomes evident on echocardiography past 10 months of age, and several mice at a year of age presented with a large LA thrombus, likely arising from blood stasis attributable to decreased atrial function, considering no evidence for atrial fibrillation, mitral regurgitation, or valve stenosis in these mice. Sorbs2-cKO mice trended toward increased RV thickness (Figure S4B) coincident with LV dysfunction; however, RV dysfunction, RV chamber dilation, or RA enlargement was not evident in echocardiographic analyses until end-stage congestive HF, in contrast to Sorbs2 global knockout mice. Gross dissection revealed that Sorbs2-cKO mice have enlarged hearts with dilated LA and LV. Four-chamber gravimetric analyses of WT and Sorbs2-cKO hearts euthanized at 48 weeks of age indicate that loss of Sorbs2 causes selective significant increases in LA mass (Figure S4C). Time-course analysis of atrial size shows that Sorbs2-cKO mice have significantly increased total atrial size (total atria mass normalized to body weight) as early as 3 to 5 months of age (Figure S4D), with substantial increases after 30 weeks of age (Figure 3D). This increase is primarily driven by LA mass versus RA or biatrial masses (cKO regression,  $r^2=0.596$ ,  $P=2e^{-4}$ ) (Figure S4E). Total ventricular mass is significantly correlated with the increased atrial mass (cKO regression,  $r^2=0.479$ ,  $P<1e^{-4}$ ) (Figure S4F); however, the magnitude of ventricular hypertrophy is substantially less (Figure 3E), reaching significance after 50 weeks (Table S5). Notably, transgenic  $\alpha$ MHC-Cre only control mice did not develop large atria or ventricles, or signs of HF (Figure 3).<sup>30</sup> Coincident with worsening cardiac structure and function, Sorbs2-cKO mice exhibit shortened lifespans, with premature death starting at  $\approx$ 1 year of age (Figure 3F), after ventricular pump function fails and mice develop pericardial and pleural effusions and ascites, indicative of congestive HF. Altogether, these data indicate that Sorbs2-cKO mice develop progressive DCM phenotype with systolic dysfunction, cardiac remodeling, and premature death.

### Cardiomyocyte-Specific Sorbs2 Knockout Mice Have Abnormal Cardiac Electrophysiology Without Atrioventricular Block

Given the prominent localization of Sorbs2 at ICDs, we hypothesized that loss of cardiomyocyte Sorbs2 may disrupt cardiac electrophysiology via initiation or

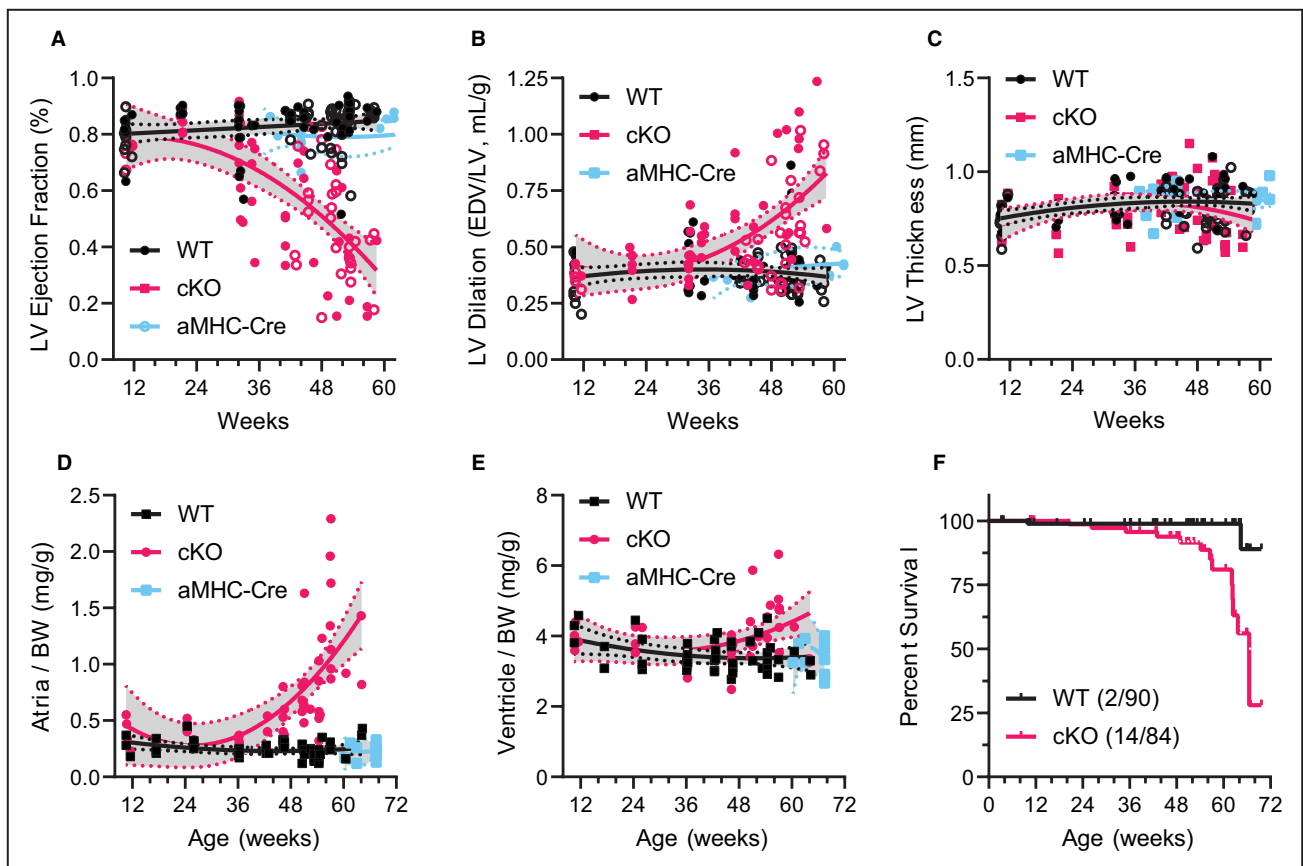


**Figure 3. Cardiomyocyte-specific Sorbs2 knockout mice develop age-related systolic dysfunction, cardiac remodeling, and premature death.**

**A through C,** Quantification of echocardiography-derived cardiac function over time, including left ventricular (LV) ejection fraction (**A**), indexed LV dilation (LV end-diastolic volume [EDV] divided by LV mass) (**B**), and LV thickness (long-axis view, septum, avoiding papillary muscles) (**C**); N=74/118 (wild type [WT]), N=55/93 (cardiomyocyte-specific knockout [cKO]), and N=12/48 ( $\alpha$ -myosin heavy chain promoter driving Cre recombinase [ $\alpha$ MHC-Cre]), N=mice/measurements, some are serial echocardiography on mice over time. Dots represent individual echocardiography/mice (solid=male, and open=female), and trendline shows a LOESS nonlinear regression fit across the mix-sex cohort, with 95% CI shaded gray. **D and E,** Postethanasias gravimetric analysis of cardiac tissue normalized to body weight (BW), including atria (**D**) and ventricle (**E**); N=55 (WT), N=46 (cKO), and N=12 ( $\alpha$ MHC-Cre), N=male mice. *P* values indicate difference between WT and cKO curves analyzed using 2-way ANOVA with Sidak multiple comparisons testing the interaction between age and genotype (see Table S5). **F,** Survival curve in mix-sex cohorts showing premature death of Sorbs2-cKO mice (median survival=66.57 weeks). Deaths (down steps) represent mice found dead in pen. Censored data (up ticks) represent mice euthanized for experiments. Death curves are significantly different using a log-rank test (Mantel-Cox method), N=90 (WT) and 84 (cKO),  $\chi^2=11.57$ , and  $P=7e^{-4}$ . Total number of deaths are noted in parentheses. LOESS indicates locally weighted smoothing.

conduction of electrical signals through the heart. We recorded surface ECGs in WT control and Sorbs2-cKO mice from 3 months through 1 year of age (Figure 4A and 4B). Collectively, these data reveal that loss of Sorbs2 in cardiomyocytes causes an obvious bifid P-wave morphology in all 3 leads (Figure 4B) with increases in P-wave duration (Figure 4C) and P-wave amplitude (Figure 4D), starting at 3 months and worsening with age. There was no change, however, in PR interval (Figure 4E). In Sorbs2-cKO hearts, QRS duration is increased (Figure 4F) and R amplitude is reduced (Figure 4G). Heart rates did subtly increase in Sorbs2-cKO mice (derived from R-R intervals; Figure 4H), perhaps to compensate cardiac output. Overall, the electrocardiographic morphologies in Sorbs2-cKO

mice suggest slow conduction in the atria (increased P-duration) and slow conduction in the ventricles (increased QRS and decreased R-amp); however, major conduction defects (ie, atrioventricular block) or significant tachyarrhythmias and bradyarrhythmias, including atrial fibrillation and ventricular tachycardia, were not found. Instead, the slow atrial conduction and abnormal P-wave morphology may reflect left atrial enlargement (Figure S4C through S4F), a common cause of bifid P-waves in clinical practice (ie, P mitrale).<sup>31</sup> Together, these data show that Sorbs2-cKO mice may have abnormal electrophysiology within the atria and ventricles, perhaps attributable to structural remodeling, without showing significant atria-to-ventricle conduction deficiencies (ie, atrioventricular block).

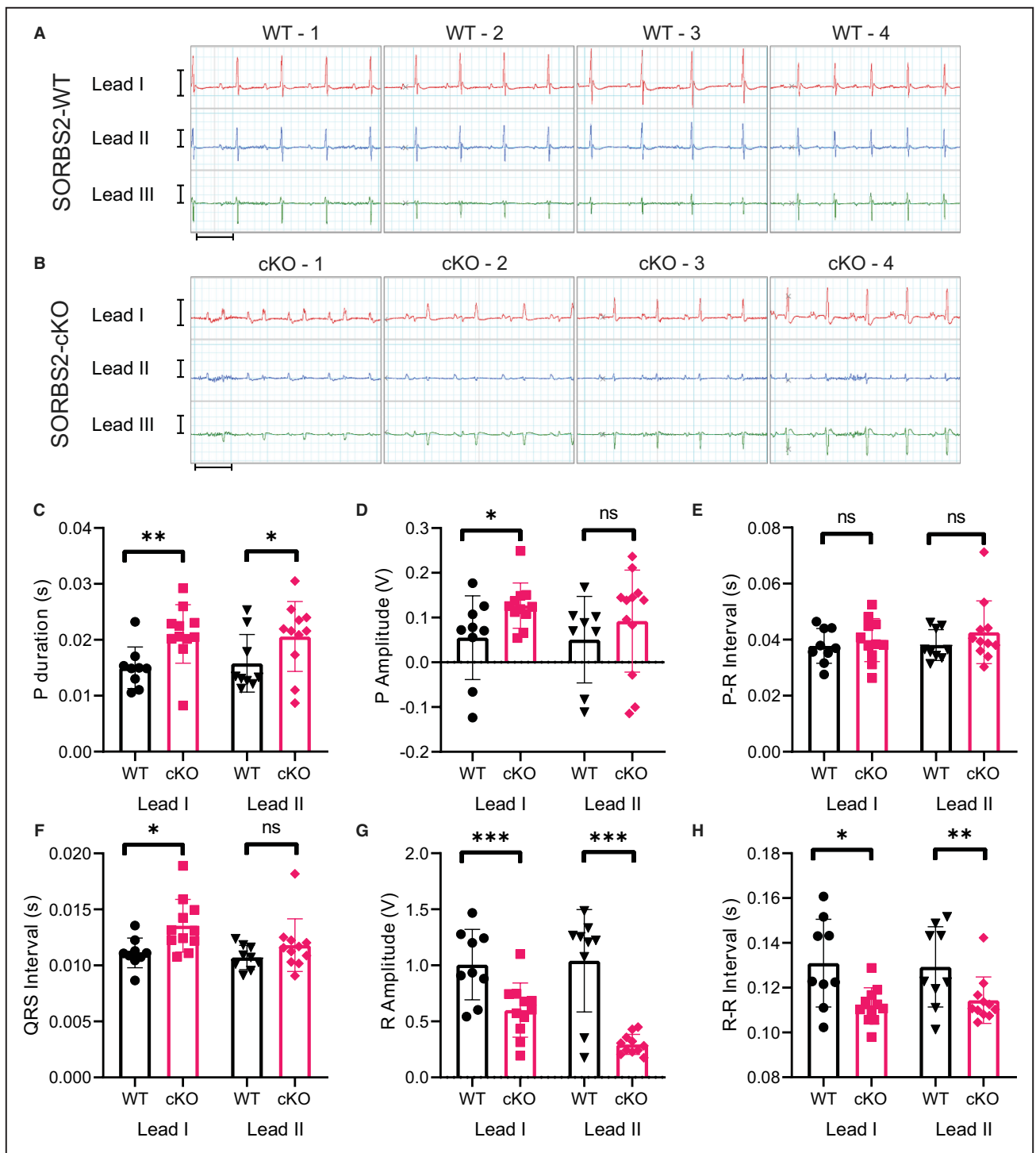


**Figure 4. Cardiomyocyte-specific Sorbs2 knockout mice (Sorbs2-cKO) display both atrial and ventricular conduction deficiencies without atrioventricular block.**

**A and B,** Representative multilead surface ECG recordings from Sorbs2-wild-type (WT) (**A**) and Sorbs2-cKO (**B**) mice aged  $\approx 12$  months old. Sorbs2-cKO mice maintain sinus rhythm but show obvious bifid P-waves, increased P-wave and QRS duration, and decreased R-wave amplitude. Y-scale=1 V, X-scale=100 ms. **C through H,** Quantification of the indicated ECG parameters from WT and cKO mice aged  $\approx 3$  months old. Dots represent individual mice with mean $\pm$ SEM, N=9 (WT) and N=11 (cKO), significance from *t*-test comparing WT and cKO for lead-I or lead-II. Ns indicates not significant. \**P*<0.05, \*\**P*<0.01, and \*\*\**P*<0.001.

### Cardiomyocyte-Specific Sorbs2 Knockout Mice Exhibit Age-Related Reductions in Cardiac and Myofiber Contractility

Sorbs2 is localized within cardiomyocytes at intercalated disks, Z-disks, and costameres, where it primarily cross-links cytoskeletal components and associated signaling complexes. Our data show that cardiomyocyte-specific loss of Sorbs2 in mice leads to a clear DCM phenotype by 1 year of age. Given that loss of Sorbs2 may weaken the cardiomyocyte cytoskeletal architecture, we hypothesized that Sorbs2-cKO mice hearts would have reduced

contractility, before detectable systolic dysfunction on echocardiography. To test this, we catheterized ≈25-week-old mice and measured LV hemodynamics at baseline and during a dobutamine infusion (dose range, 2–12 ng/g per minute). WT control mice (fl/fl, Cre negative) increased cardiac contractility (shown as maximum change in LV pressure over time) coincident with increasing dobutamine concentrations, whereas Sorbs2-cKO mice did not (Figure 5A). Both genotypes similarly increased heart rate in response to dobutamine challenge (Figure S5A), indicating that adrenergic signaling was intact in Sorbs2-cKO hearts. At baseline, cardiac contractility was not different among

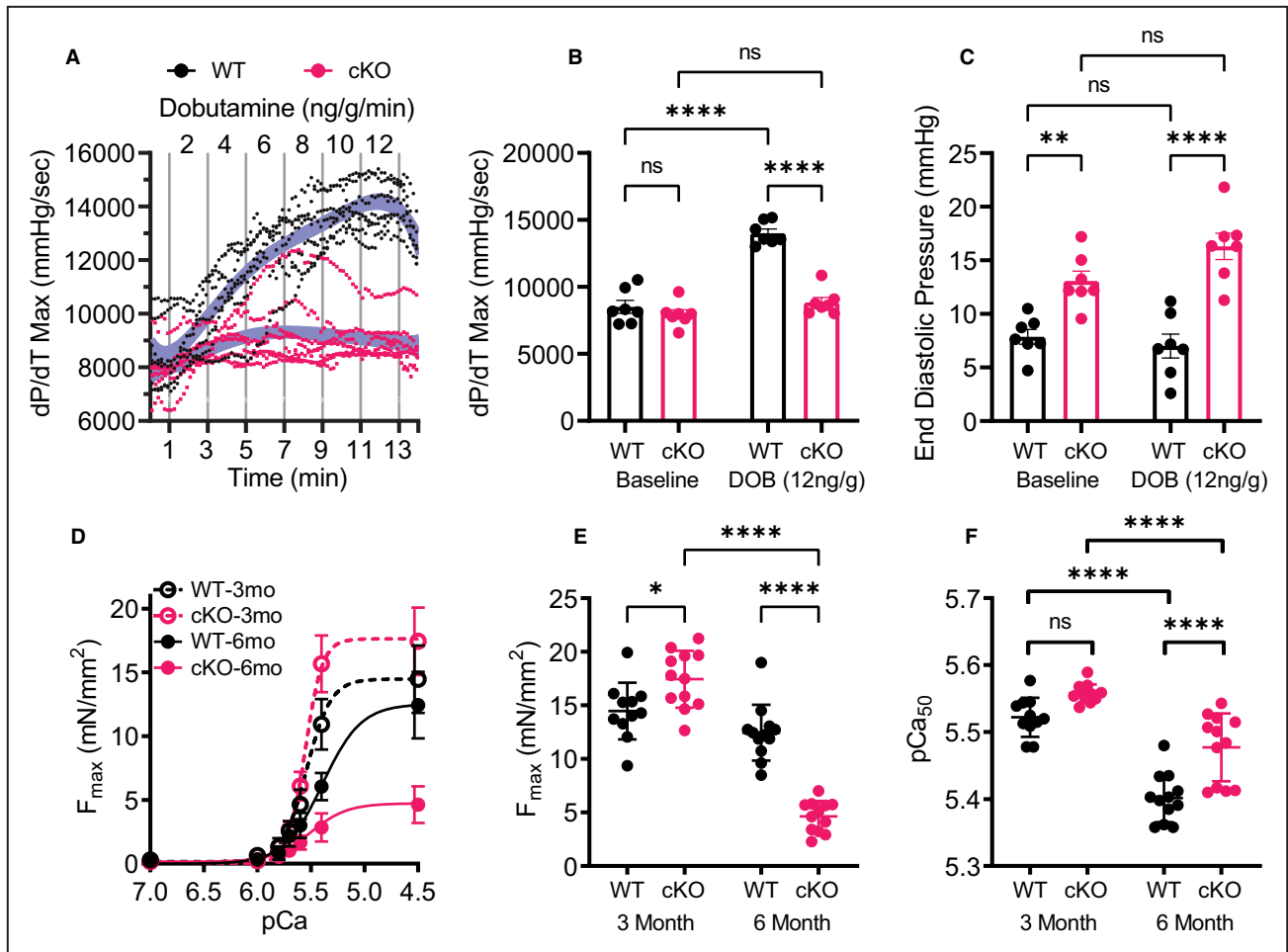


**Figure 5. Cardiomyocyte-specific Sorbs2 knockout mice (Sorbs2-cKO) have severe contractile dysfunction.**

**A**, Cardiac contractility (maximum change in left ventricular [LV] pressure over time [dP/dT Max]) derived from LV catheterization and stepped infusion of dobutamine (DOB; 2 minutes per dose indicated on top) in ≈6-month male mice. Dots show 10-second average for individual mice (n=7 mice per group). The blue shading denotes a LOESS nonlinear regression ±95% CI and are significantly different ( $P<1e^{-4}$ ) via repeated measures 2-way ANOVA with Sidak multiple comparisons testing the interaction between age and genotype. Final 30-second average per DOB dose (12 ng/g per minute) for dP/dT Max (**B**) and end-diastolic pressure (**C**). **D**, Isometric calcium concentration (pCa)–tension curves generated from skinned LV myofibers male mice at 3 and 6 months old. Each data point represents the mean±SEM of 11 to 12 myofibers isolated from 4 different mice per group (2–3 fibers per mouse). Trendline denotes a least-squares fit to sigmoidal dose-response curve with variable slope. **E**, Maximum developed tension (Fmax; mN/mm<sup>2</sup>). **F**, Calcium sensitivity (pCa<sub>50</sub>; M) was calculated from isometric pCa-tension curves. **B**, **C**, **E**, and **F**, Dots show individual data (mice or myofibers) with mean±SEM; statistics acquired using 1-way ANOVA with Sidak post hoc test comparing selected groups (each comparison shown on plot). LOESS indicates locally weighted smoothing; Ns, not significant; and WT, wild type. \* $P<0.05$ , \*\* $P<0.01$ , and \*\*\*\* $P<0.0001$ .



mice; however, control mice achieved a sustained increase in maximum change in LV pressure over time, with peak contractility  $\approx 1400$  mm Hg/s at 12 ng/g per minute dobutamine, the highest dose tested (Figure 5B). Contractility was significantly reduced in Sorbs2-cKO mice with a peak at 8 ng/g per minute and remained blunted through 12 ng/g per minute to  $\approx 9000$  mm Hg/s (Figure 5B). Cardiac relaxation (indicated by minimum change in LV pressure over time) was not different between groups at baseline but was significantly blunted in Sorbs2-cKO mice during dobutamine challenge (Figure S5B). In addition, at baseline, Sorbs2-cKO hearts showed increased end-diastolic pressure, which further increased with dobutamine (Figure 5C), suggesting basal diastolic dysfunction. Surface electrocardiographic measurements were also recorded from both WT control and Sorbs2-cKO mice during the dobutamine challenge. Although bifid P-waves and increased P-durations were present in Sorbs2-cKO mice, they maintained normal sinus rhythm with no signs of atrial or ventricular arrhythmias or atrioventricular block (Figure S5C through S5F). Dobutamine challenge data suggest that Sorbs2-cKO hearts have intrinsic defects in contractility, causing insufficient contraction within cardiomyocytes. To test this, calcium-induced isometric tension was measured in permeabilized LV myofibers from WT (fl/fl, CRE negative) and Sorbs2-cKO mouse hearts at 3 or 6 months of age (Figure 5D). Contrary to our hypothesis, these data show that myofibers from 3-month-old Sorbs2-cKO hearts do not have reduced maximal force generation, nor reduced calcium sensitivity, but instead show increased maximum tension (Figure 5E and 5F), perhaps attributable to compensatory mechanisms. In contrast, LV myofibers from 6-month-old Sorbs2-cKO mice show a significant reduction in tension development, with minor differences in calcium sensitivity (Figure 5E and 5F). These findings indicate that before systolic dysfunction, Sorbs2-cKO mice have impaired myofiber contractility, consistent with our dobutamine challenge findings. Altogether, the data support that appropriate cardiomyocyte excitation remains intact during  $\beta$ -adrenergic stress in Sorbs2-cKO mice; however, these mice fail to increase cardiomyocyte mechanics and/or couple excitation to contraction.

### Molecular Changes in Cardiomyocyte-Specific Sorbs2 Knockout Hearts

Sorbs2-cKO mice develop age-dependent DCM with abnormal electrophysiology and contractility; however, the underlying molecular mechanisms remain undefined. We explored several possibilities to determine how loss of Sorbs2 over time causes HF in mice, focusing on ICDs, ion channels, calcium handling,

and cytoskeletal/sarcomeric proteins. Relevant summarized time-course western blot data (done on WT and Sorbs2-cKO heart lysates collected at 3, 6, and 12 months of age) are shown in Figure 6A through 6D, and representative data are shown in Figure S6A through S6D.

### Cardiomyocyte-Specific Sorbs2 Knockout Mice Retain ICD Protein Expression and Localization

Prior work suggests that Sorbs2 is an RNA-binding protein that is required to stabilize Gja1 (connexin 43 [Cx43]) mRNA and maintain ICD structure.<sup>7,29</sup> To assess if Sorbs2-cKO hearts have less Gja1/Cx43 or altered expression of other ICD proteins, we measured protein levels via western blot (Figure 6A and Figure S6A). Despite prior observations that global Sorbs2 knockout hearts show a >90% reduction in cardiac Cx43 protein levels,<sup>7</sup> surprisingly, Sorbs2-cKO hearts maintain normal Cx43 expression from 3 to 12 months of age. In addition, no other ICD proteins, including connexin 40 (Gja5), N-cadherin (Cdh2),  $\gamma$ -catenin (Jup), tight junction protein 1 (Tjp1/Zo1), and  $\beta$  catenin (Ctnnb1), were found to be consistently altered. Overall, these data support that loss of Sorbs2 in cardiac myocytes does not grossly perturb expression of key ICD proteins and further contradicts (along with RNA sequencing data described above) the notion that Sorbs2 is an RNA-binding protein that promotes expression of Gja1/Cx43 or other ICD proteins in cardiomyocytes.

Cardiac conduction and contractile deficits are linked to mutations in cytoskeletal and ICD genes, and derangements in cardiomyocyte cytoskeletal architecture. Global Sorbs2 knockout mice show overt downregulation of Gja1/Cx43 and mislocalization of other ICD proteins.<sup>7,29</sup> To test if cardiomyocyte-specific loss of Sorbs2 causes similar aberrations, we stained cytoskeletal proteins in longitudinal heart sections from WT control and Sorbs2-cKO mice at 8 months of age (Figure S7A and S7B). Cell membranes stained with wheat germ agglutinin show myocytes of consistent size and shape in both genotypes. WT hearts show Sorbs2 colocalized with  $\beta$ -catenin (Ctnnb1) at ICD structures and in striations along lateral membranes, consistent with costamere structures (Figure S7A). Sorbs2-cKO hearts lose immunoreactivity for Sorbs2 at ICDs and costameres; however, cardiomyocytes maintain normal Ctnnb1 localization at ICDs (Figure S7B). Staining of heart sections with phalloidin, and antibodies against sarcomeric actinin, vinculin (Vcl), and Gja1/Cx43, also showed consistent cardiomyocyte size and sarcomere distribution, and remarkably, Vcl and Gja1/Cx43 expression and localization at costameres and/or ICDs were no different between control and Sorbs2-cKO hearts (Figure S7C through S7F).

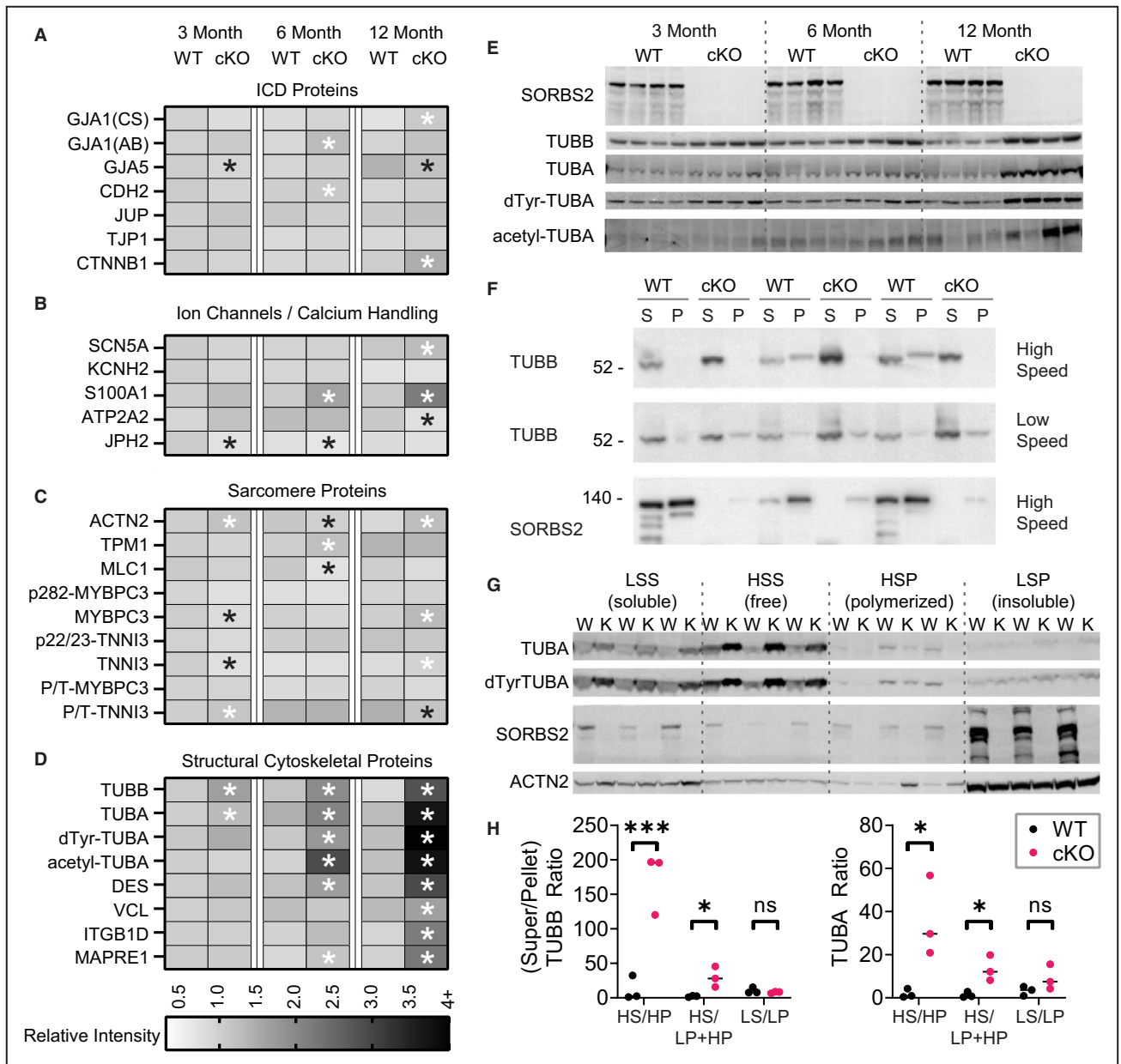


**Figure 6. Cardiomyocyte-specific Sorbs2 knockout mice (Sorbs2-cKO) have dysregulated cytoskeletal protein expression.**

**A** through **D**, Heat maps show analysis of protein expression from wild-type (WT) and Sorbs2-cKO cardiac lysates at 3, 6, and 12 months of age. Each box represents the mean integrated intensity, normalized to loading control and expressed relative to 3-month WT; n=4 mice per group. Significant differences ( $P<0.05$ ) denoted with asterisk (black for downregulated, and white for upregulated) overlay on the heat map, were acquired using *t*-test comparing cKO with WT at each age. Raw western blots are shown in Figure S6. Heat maps are organized by ICD proteins (**A**), ion channels and calcium handling proteins (**B**), sarcomere proteins (**C**), and structural cytoskeletal proteins (**D**). **E**, Western blots show Sorbs2-cKO hearts have significant, early, and sustained expression of microtubule proteins (quantified data in **D**). **F**, Microtubule fractionation assay from cardiac tissue for male mice aged 16 weeks shows decreased level of polymerized Tubb and increased levels of free Tubb high-speed fractions from Sorbs2-cKO hearts. Sorbs2 is shown to be present in high-speed, polymerized microtubule fraction. **G**, Microtubule fractionation assay also shows decreased level of polymerized microtubule proteins (Tuba and dTyr-Tuba) and increased levels of free microtubule protein high-speed fractions from Sorbs2-cKO hearts. Note the majority of Sorbs2 is retained in the low-speed pellet, representing 1% Triton-X insoluble proteins, along with sarcomeric actinin and likely other cytoskeletal proteins. **H**, Ratiometric quantitation of free/polymerized Tubb and Tuba. Dots represent individual mice with mean; statistics acquired using *t*-test comparing cKO with WT. \* $P<0.05$ , \*\*\* $P<0.001$ . AB indicates abclonal; CS, cell signaling; H, high speed; L, low speed; ns, not significant; P, pellet; and S, supernatant.

## Ion Channels and Calcium Handling

### Ion Channels

Sorbs2-cKO mice have abnormal cardiac electrophysiology with increased P-wave duration and amplitude, which may be attributable to an atrial conduction deficiency, abnormal depolarization, or increased atrial size. The voltage-gated sodium channel  $\text{Na}_v1.5$  (encoded by *Scn5a*) is a primary contributor to cardiac depolarization,<sup>32</sup> *Sorbs2* is known to cluster membrane-associated complexes<sup>33,34</sup> and predicted to bind  $\text{Na}_v1.5$ , and coexpression analyses strongly support that *Sorbs2* and *Scn5a* expressions are highly correlated. Thus, we tested whether loss of *Sorbs2* decreases *Scn5a* expression or regulates  $\text{Na}_v1.5$  activity. Unexpectedly, western blot analysis shows that 12-month-old *Sorbs2*-cKO hearts trend toward increased  $\text{Na}_v1.5$  expression compared with WT mice, coinciding with the DCM phenotype, and end-stage HF (Figure 6B and Figure S6B). Expression of *Kcnh2* (encodes the cardiac inward rectifying potassium channel mERG, which is primarily responsible for cardiac repolarization) is also unchanged in *Sorbs2*-cKO hearts. *Scn5a* and *Kcnh2* encode 2 of several ion channels downregulated in global *Sorbs2* knockout mice and purported to be direct targets for *Sorbs2* RNA-binding activity<sup>29</sup>; however, our data contradict this conclusion.

Electrophysiology experiments were done using NRCMs transiently transfected with expression plasmids encoding either *Sorbs2* (mouse cardiac-specific isoform; Figure S2A; “our clone”) or green fluorescent protein as control and assessed for endogenous sodium current. In parallel, NRCMs were transiently transfected with nontargeting control or *Sorbs2* siRNAs for loss-of-function comparisons. The resulting data show that  $\text{Na}_v1.5$  channel current density is not affected by overexpression or knockdown of *Sorbs2* (Figure S8C through S8F). Together, these data suggest that potential *Sorbs2*-mediated regulation of  $\text{Na}_v1.5$  expression or activity likely does not account for the conduction deficits observed in *Sorbs2*-cKO mice.

### Calcium Handling

*Sorbs2*-cKO mice have abnormal contractility that may be attributable to dysregulated calcium handling/signaling in cardiomyocytes. We assessed the potential for *Sorbs2*-cKO hearts to exhibit decreased expressions of S100a1 (multifactorial calcium-binding protein), *Atp2a2* (*Serca2a*, calcium transporter), and *Jph2* (junctophilin 2, cardiac dyad scaffolding protein). *Jph2* levels were only slightly decreased at 3 and 6 months, *Atp2a2* expression is decreased at 12 months (Figure 6B and Figure S6B), and no changes in the ratio of phosphorylated/total Tnni3 and *Mybpc3*, a hallmark of calcium-dependent posttranslational regulation, were found

in *Sorbs2*-cKO hearts (Figure 6C and Figure S6C). Unexpectedly, we found that myocardial S100a1 expression is increased 2- to 3-fold in *Sorbs2*-cKO mice at 6 and 12 months of age (trending at 3 months); this is interesting and perhaps another indication of compensation, considering that S100a1 bolsters cardiac function in the setting of HF.<sup>35,36</sup>

To begin addressing whether decreased *Sorbs2* expression in cardiomyocytes alters calcium, we transiently transfected NRCMs with siRNA against *Sorbs2* and measured whole-cell basal calcium. Within 48 hours, *Sorbs2* knockdown led to significant increases in whole-cell calcium concentrations (Figure S8B), which complements published findings showing that short-term overexpression of *Sorbs2* decreases peak intracellular calcium; however, the latter was deemed to occur secondary to *Sorbs2*-mediated densification of microtubule networks, thus we focused on potential structural derangements.<sup>8</sup>

### Sarcomere Proteins

We assessed if loss of cardiomyocyte *Sorbs2* alters expression or phosphorylation of sarcomeric proteins (Figure 6C and Figure S6C). Levels of sarcomeric proteins and the calcium-dependent phosphorylation status (ie, ratio of phosphorylated/total) of p22/23-Tnni3 and p282-Mybpc3 were not overtly different in WT and *Sorbs2*-cKO heart at 3, 6, or 12 months of age. Although some statistically significant differences were found, these were typically subtle in magnitude and did not show consistent or progressive alteration across time points, supporting that loss of *Sorbs2* does not cause overt stoichiometric changes in sarcomeric contractile proteins. Staining of actin fibers in heart sections with phalloidin and antibodies against sarcomeric actinin showed consistent cardiomyocyte size and sarcomere distribution between control and *Sorbs2*-cKO hearts (Figure S7C and S7D). Together, these data support that sarcomeric derangements and modified calcium sensitivities are not likely culprit triggers for cardiac dysfunction in *Sorbs2*-cKO mice, suggesting that reduced force generation could be linked to altered cytoskeletal structures (eg, microtubules, intermediate filaments, and associated cross bridges and anchoring sites).

### Sorbs2-cKO Mice Exhibit Derangements in Cardiac Structural Cytoskeletal Protein Expression and Destabilized Microtubules

Beyond the potential for ICD derangements, recent reports indicate that *Sorbs2* binds cytoskeletal proteins, including tubulins, and regulates microtubule dynamics in cardiomyocytes.<sup>8,37</sup> Indeed, across all of the proteins/pathways that we assayed by western blot,

the most profound, earliest, and consistent changes occurred with microtubule proteins, with Sorbs2-cKO hearts showing significantly increased levels of  $\beta$ -tubulin (Tubb),  $\alpha$ -tubulin (Tuba) deetyrosinated-Tuba and acetylated-Tuba (Figure 6D and 6E) at 3 months of age, and persisting through 6 and 12 months. The microtubule adaptor protein EB1 (Mapre1) and integrin protein Itgb1d, which modulate microtubule dynamics, increased in similar manner. Other noncontractile cytoskeletal proteins, including desmin and Vcl, were also elevated after 6 or 12 months, respectively (Figure 6D and Figure S6D); however, these are common downstream hallmarks of contractile dysfunction found in most cardiomyopathies.

To determine if cardiomyocyte-specific loss of Sorbs2 alters microtubule polymerization/stabilization, we performed western blot analyses after subcellular fractionation of WT and Sorbs2-cKO heart lysates from  $\approx$ 16-week-old mice. This revealed that Sorbs2-cKO samples have significantly increased free Tubb and decreased polymerized Tubb (Figure 6F and 6H). Tuba and deetyrosinated Tuba also show increased free/polymerized ratio in Sorbs2-cKO samples (Figure 6G and 6H), suggesting defective microtubule polymerization or stabilization. Although the vast majority of Sorbs2 in these samples remained in the low-speed pellet, likely representing detergent insoluble proteins, including other cytoskeletal components (see sarcomere actinin for comparison), some Sorbs2 was notably found in high-speed pellet fractions (Figure 6F and 6G), consistent with Sorbs2 attachment to polymerized microtubules. Altogether, these data provide a loss-of-function complement to published findings showing that Sorbs2 overexpression promotes microtubule polymerization/stability and suggest that early and persistent changes in microtubule proteins could be at the root of cardiac dysfunction in Sorbs2-cKO mice.

### Summary of Molecular Changes in Sorbs2-cKO Hearts

Overall, our investigations into potential underlying mechanisms do not indicate significant redistribution of ICD proteins, rearrangement of sarcomeres, or dysregulated expression of ICD proteins in mice with cardiac-specific loss of Sorbs2. This is consistent with others who show that although Sorbs2 is a component of tight and adherens junctions in epithelial cells, Sorbs2 loss does not affect the assembly, structure, or function of these junctions.<sup>38</sup> Rather, our findings support that decreasing heart function, deemed by significantly reduced LV EF, in Sorbs2-cKO mice is preceded by early abnormalities in microtubule dynamics, which associates with subtle and transient downregulation of contractile cytoskeleton proteins in the sarcomere and subsequent upregulation of cytoskeletal structural

proteins, likely as a compensatory mechanism to bolster the cytoskeletal architecture. Although we are unable to completely rule out changes in cardiomyocyte calcium handling as causative, these changes likely occur secondary to microtubule derangement and subsequent Jph2 redistribution.<sup>8</sup> Rather than Sorbs2 acting as an RNA-binding protein in cardiomyocytes to regulate ion channels and ICD proteins, our findings herein are consistent with the more established role for SORBS proteins as cytoskeletal cross-linking adapter proteins.

### The SORBS Family and Clinical Genetic Associations

Our results indicate that Sorbs2 plays an essential role in maintaining normal cardiac function and is consistently dysregulated in clinical cardiomyopathy and rodent models of cardiac stress. To further explore the potential clinical relevance of Sorbs2, and other SORBS family members, we performed database and literature searches to assess if genetic variations in SORBS genes are associated with cardiac-related clinical phenotypes (results summarized in the Table). GWAS catalog search yielded a Sorbs2 variant associated with serum cardiac troponin T levels,<sup>23</sup> a predictor of cardiovascular disease risk. Interestingly, this same variant is significantly associated with paroxysmal ventricular tachycardia in UK Biobank GWAS data, summarized by PheWeb.<sup>24</sup> With relevance to our findings in Sorbs2-cKO mice, query of the Cardiovascular Disease Knowledge Portal indicated strong associations for both Sorbs1 and Sorbs2 variants with P-wave interval/duration, the former of which was previously reported,<sup>26</sup> and is also linked to cardiac arrest in UK Biobank GWAS data. In addition, Cardiovascular Disease Knowledge Portal revealed a Sorbs2 variant associated with P-wave terminal force,<sup>21</sup> a known indicator of LA enlargement, and this variant is significantly associated with DCM in published GWAS data<sup>22</sup> and with decreased Sorbs2 expression in human cardiovascular tissue samples.<sup>3</sup> Although many of these associations are of subthreshold significance by GWAS standards (ie, 5e-8), in sum, these and other relevant associations highlighted in the Table point to the interesting possibility that genetic variations in SORBS genes influence the onset and progression of several cardiovascular-related clinical phenotypes, with several notable instances that are consistent with our observations in Sorbs2-cKO mice (eg, P-wave alterations, LA enlargement, and DCM).

## DISCUSSION

Beyond the field's focus on the cytoskeletal/sarcomeric proteins themselves, this work highlights and reiterates



an important role for cytoskeletal adapter proteins in the onset and development of cardiomyopathy. There has been mounting interest in the functions of SORBS proteins in cardiac biology and disease, yet their roles specifically in cardiomyocytes, where they are most highly expressed, have not been assessed using conditional gene deletion mouse models, or relevant transgene sequences (ie, cardiac Sorbs2 transcript isoforms). To address this, we generated and characterized mice with cardiac-specific loss of Sorbs2, the most abundantly expressed SORBS family member in heart. In addition, we interrogated available bioinformatic data sets to examine Sorbs2 dysregulation in mouse models and patients with HF and whether SORBS genetic variants are associated with cardiac phenotypes. Overall, our studies provide key insights into the critical role for Sorbs2 in maintaining cardiac structure/function and highlight its potential clinical relevance.

In summary, Sorbs2 is consistently upregulated in humans with ischemic and idiopathic cardiomyopathies, and in experimental animal models of these diseases. Sorbs2 predominantly localizes to the intercalated disc and along sarcomeres at Z-discs, particularly adjacent to the lateral membrane at costameres in cardiomyocytes (Figure 7). Sorbs2-cKO mice exhibit atrial and ventricular conduction defects, underlying diastolic dysfunction, develop progressive systolic dysfunction starting after 6 months of age, and die

with congestive HF after 12 months of age. Systolic dysfunction is coincident with severely impaired cardiac contractility attributable in part to a failure to generate adequate mechanical tension in myofibers. Interrogation of cytoskeletal structures indicates that loss of Sorbs2 in cardiomyocytes does not significantly impair expression or distribution of ICD proteins, but instead leads to defective microtubule polymerization/stability and compensatory upregulation of structural proteins ( $\alpha$ -tubulin and  $\beta$ -tubulin, desmin, and vinculin) (Figure 7). Our data, in conjunction with prior literature, support that Sorbs2 is an adapter protein that functions to maintain the structural integrity of the cardiomyocyte cytoskeleton by strengthening interactions between microtubules and other structural proteins at cross-link sites.

### Microtubule and Cytoskeletal Proteins Relevant to Cardiac Function

Our work herein may further direct research efforts to better understand how SORBS proteins regulate microtubule dynamics in cardiomyocytes, and beyond. Sorbs2 can bind to Tubb and enhance microtubule polymerization,<sup>8,37</sup> and our data complement these findings in showing that Sorbs2-cKO hearts have reduced levels of polymerized microtubules despite substantially increased tubulin protein levels, before systolic dysfunction. Other studies of age-related

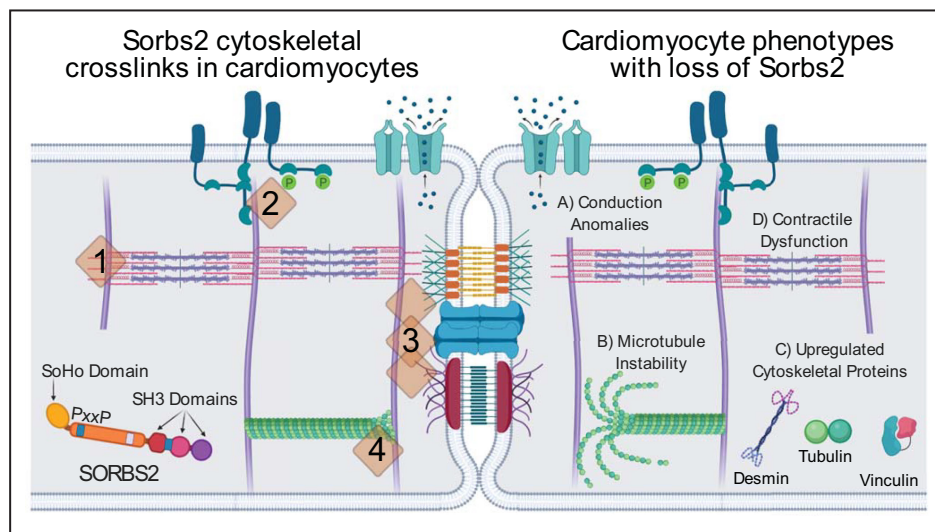


**Figure 7. Theoretical model of Sorbs2 functional interactions in cardiomyocytes.**

Sorbs2 is a cytoskeletal adaptor protein that facilitates diverse protein-protein interactions through its sorbin homology (SoHo), SH3 domains, and proline-rich motifs (PxxP). Sorbs2 functional interactions in cardiomyocytes include (1) z-discs, (2) costameres, (3) intercalated discs, and (4) microtubules, through cross-link binding with intermediate filaments, actinin, and other adaptor proteins, and cell signaling complexes. Age-dependent dilated cardiomyopathy occurs after cardiomyocyte-specific deletion of Sorbs2, which broadly weakens these cytoskeleton structures, and manifests as early conduction anomalies, in part, caused by atrial enlargement (A), microtubule instability (B), increased cytoskeletal protein expression (C), and eventually contractile dysfunction leading to heart failure (D). Created with [BioRender.com](https://www.biorender.com).

cardiomyopathies in mice reported decreased microtubule polymerization and aberrant microtubule dynamics coincident with HF.<sup>39,40</sup> Prior work also found increased microtubule abundance in human and animal models of dilated HF, ischemic cardiomyopathy, and cardiac hypertrophy,<sup>41–44</sup> with particular emphasis on elevations in detyrosinated Tuba, which increases binding of microtubule-associated proteins on plus ends and contributes to increased cell stiffness,<sup>45,46</sup> resisting both compressive and stretching forces.<sup>47,48</sup> Future work will be needed to determine if the microtubule changes observed in Sorbs2-cKO hearts are a primary consequence of Sorbs2 loss or a proximal adaptation to early systolic dysfunction. Although we observed changes in microtubule abundance in Sorbs2-cKO hearts before systolic dysfunction, suggesting a causal link, others have proposed that rewiring of microtubule and desmin networks may be an early-disease change before end-stage HF requiring transplant.<sup>42</sup> Although we cannot be certain whether the microtubule changes are secondary to cytoskeletal weakening attributable to loss of Sorbs2 cross-linking, temporary downregulation of sarcomere components, or whether Sorbs2 directly modifies the microtubules, our data in conjunction with published data on SORBS proteins support reasonable speculation that these may underlie the onset of HF in Sorbs2-cKO mice.

Prior studies also indicate that the nonsarcomeric cytoskeleton is necessary for normal cardiomyocyte contractility, tension sensing, and signal transduction.<sup>49</sup> Considering the established role for SORBS proteins as actin filament cross-linking adaptor proteins, one interesting speculation is that Sorbs2 is critical for maintaining connections among the structural cytoskeleton (microtubules, desmin, Actn2, and Vcl) and the contractile cytoskeleton (sarcomeres) at cardiomyocyte z-discs, costameres, and ICDs. Recently, an immunoprecipitation mass spectrometry-based proteomics approach was used to confirm Sorbs2 protein interactions with *Tubb2a*, desmin, Actn1/2, Vcl, and Myh7/9 in heart and human embryonic stem cell-derived cardiomyocytes,<sup>37</sup> perhaps suggesting a causal relationship between loss of Sorbs2 and dysregulation of these proteins. Although we know these important connections are critical for coordinating cardiomyocyte excitation, contraction, and relaxation mechanics, the molecular mechanisms for how individual cardiomyocytes sense changes in mechanical load and respond with compensatory changes in cytoskeletal proteins need further investigation. We speculate that cardiomyocyte loss of Sorbs2 weakens the cross-linking interactions of tubulin, desmin, actin, and actinin proteins at z-discs and intercalated discs and that, over time (beat by beat), this manifests into detectable maladaptive remodeling of microtubule and intermediate filament networks, likely to increase tensile strength

and modify cardiomyocyte contraction/relaxation. If so, this weakening is likely to occur to a subtle extent (ie, difficult to measure) given the delayed manifestation of contractile dysfunction observed in Sorbs2-cKO mice at about 6 months of age (>100 000 000 heart beats).

Additional published work strongly supports our speculation that Sorbs2 cross-links the cardiomyocyte cytoskeleton through diverse protein:protein interactions (mediated by its sorbin homology and SH3 domains and proline-rich motifs) with actin, microtubules, and associated proteins, as well as enabling signal transduction pathways. Sorbs2 was originally identified as an Abl2 (also known as ARG) interacting protein through a 2-hybrid approach.<sup>50</sup> This interaction has been reconfirmed and extends to other members of both the ABL and SORBS families and dozens of other Abl interacting proteins and phosphorylation targets, including Abi1,<sup>51</sup> Cbl,<sup>52</sup> and others.<sup>53</sup> ABL family kinases are necessary for cardiac growth and development,<sup>54</sup> localize to focal adhesion and adherens junctions,<sup>55,56</sup> and exhibit multifaceted roles in the regulation of cytoskeleton proteins.<sup>57</sup> In addition to their kinase activities, Abl1 and Abl2 have non-kinase-dependent functional interactions with both actin fibers and microtubules that are sufficient to regulate the dynamics and stability of these cytoskeletal filaments.<sup>56,58,59</sup> Future work is needed to determine how Sorbs2, which itself is phosphorylated by Abl kinases<sup>50</sup> (as well as others), fits into Abl signal transduction pathways in cardiomyocytes. Beyond the Abl kinase family, other Sorbs2 interacting proteins have been identified with well-described regulatory roles in cytoskeletal biology.<sup>33</sup> The ubiquitin ligase Cbl is anchored by Sorbs2<sup>60</sup> and directly regulates microtubule polymerization.<sup>61</sup> Furthermore, large-scale protein-protein interaction studies suggest that Sorbs2 interacts with Mapre1 (also known as EB1),<sup>62</sup> which belongs to a family of microtubule-end capping adaptor proteins that interact with SH3 domains through conserved proline-rich regions.<sup>63</sup> Sorbs2 also interacts with the actin:myosin cross-linking protein Mybpc3<sup>64</sup>; however, the relationship between these and other z-disc attachments and Sorbs2 interacting proteins<sup>37</sup> remains unclear. Further and carefully designed experiments will be needed to define the cellular response to overexpression of Sorbs2 in mature cardiomyocytes as excess Sorbs2, above physiological levels, is sufficient to sequester interacting protein partners and collapse the cytoskeleton in cardiomyocytes<sup>65</sup> as well as other cell types.<sup>38</sup> This may confound the results observed when viral overexpression of Sorbs2 induced rapid HF in mice (ie, within 3 weeks).<sup>8</sup> Extensive future work will be needed to further tease apart the role for SORBS proteins in these dense cytoskeletal cross-linking networks, especially in mature cardiomyocytes, with extended consideration for the potential for altered cardiomyocyte cytoskeleton to

**Table. Unexplored Genetic Variation in *SORBS* Gene Family Underlies Cardiovascular Diseases**

rs Identifier	Phenotype	P value	Reference
Sorbs2			
rs5018568	mRNA eQTL	9e-6	3 GTEx project
	P-wave terminal force	5e-4	21 PWI GWAS
	Dilated cardiomyopathy	0.002	22 DCM GWAS
rs75898208	Plasma cTnT levels	2e-9	23 cTnT GWAS
	Ventricular tachycardia	2e-3	24 UK Biobank
rs10009306	ICD shocks	3e-4	25 GAME GWAS
	Arrhythmia	0.06	24 UK Biobank
rs182253016	Hypertensive heart disease	4e-7	24 UK Biobank
Sorbs1			
rs1410059	PR interval	7e-8	26 PR GWAS
	Cardiac arrest	0.04	24 UK Biobank
rs3193970	Sudden cardiac arrest	1e-4	27 SCA GWAS
	Cardiac arrest	0.03	24 UK Biobank
rs943346	Cardiovascular disease	6e-8	28 FINDOR
rs12221125	Systolic blood pressure	9e-9	28 FINDOR

cTnT indicates cardiac troponin-T; DCM, dilated cardiomyopathy; eQTL, expression quantitative trait loci; FINDOR, functionally informed novel discovery of risk loci; GAME, genetic arrhythmia markers for early detection; GTEx, genotype-tissue expression; GWAS, genome-wide association study; ICD, intercalated disc; PWI, P-wave indices; and SCA, sudden cardiac arrest.

influence extracellular matrix composition (eg, fibrosis, which we did not evaluate in Sorbs2-cKO mice).

### Potential Mechanisms for Altered Cardiac Electrophysiology

Whole-body constitutive loss of Sorbs2 causes lethal ARVC in mice,<sup>7</sup> and although some phenotypes are shared between the whole-body knockout and cardiomyocyte-specific knockout mice (ie, bifid P-waves, QRS waveform anomalies, HF, and death), notable discrepancies exist. Global Sorbs2 knockout mice develop an aggressive “ARVC-like” phenotype, RV dilation, and arrhythmias and die between ~4 to 6 months of age. By contrast, Sorbs2-cKO mice show slow progressing DCM phenotype, without arrhythmias despite early LA enlargement, and die between ~11 to 15 months old. Sorbs2-cKO mice also do not show severe RV dilation nor clear signs of arrhythmia or altered Cx43 expression, which was astonishingly reduced by 90% in global Sorbs2 knockout mice. Overall, global and cardiomyocyte-specific Sorbs2 knockout mice are distinct, and our work helps to clarify the specific contribution of Sorbs2 loss in cardiomyocytes to cardiac structure and function in mice and highlights important likely roles for Sorbs2 in other cell types in contributing to diverse cardiac phenotypes.

Sorbs2-cKO mice exhibit P-wave alterations that may be attributable to increased atrial size rather than atrial conduction deficiency. Clinical presentation with bifid P-waves coincides with increased left atrial size,<sup>31</sup> consistent with our observed correlations in

Sorbs2-cKO. Given the profound cytoskeletal remodeling observed in Sorbs2-cKO mice, lack of disrupted Cx43 and Na<sub>v</sub>1.5 expression, and absence of atrial fibrillation, we speculate that the P-wave changes are predominantly of structural origin. Many potential physiological mechanisms could explain increased left atrial size, including cardiac development, structural remodeling affecting atrial compliance (hypertrophy/fibrosis), or hemodynamics (left atrial pressure overload attributable to poor ventricular contractility). Future work will need to directly investigate the contribution of Sorbs2 expression in these and other atrial mechanisms.

Atrial-to-ventricular conduction defects (ie, atrioventricular block) or irregular heart rates were not present in Sorbs2-cKO mice but were in global knockout mice. Although the exact mechanism by which Sorbs2 controls cardiac conduction remains unknown, our data contest that this does not involve potential post-transcriptional regulation of Scn5a/Na<sub>v</sub>1.5, Kcnh2/mERG, or Gja1/Cx43 through Sorbs2 RNA-binding functions in cardiomyocytes, as suggested by prior global Sorbs2 knockout mouse studies.<sup>7,29</sup> It is possible that the severe reduction of myocardial Gja1/Cx43 (and other ion channel expression and function) in global Sorbs2 knockout mice occurs secondary to more severe HF, and is not mechanistically related to Sorbs2 expression.<sup>66</sup> This notion is further supported by the fact that Sorbs2 RNA-binding properties occur through its conserved ZnF-C2H2 domain located in human exon 35 (mouse exon 23)<sup>67,68</sup>; and notably, this exon is restricted to alternate transcripts that are expressed in specific cell types (ie, neuronal tissues) and

largely absent from cardiomyocytes and heart tissues (Figure S2A and S2B). It is worth reiterating that previous gain-of-function studies<sup>29</sup> that demonstrate RNA-binding activity of Sorbs2 in cardiomyocytes used a neuronal Sorbs2 transcript harboring the RNA-binding domain.<sup>9</sup> Beyond this, we further speculate that the more aggressive arrhythmia phenotypes in global Sorbs2 knockout mice may result from contributions of key Sorbs2 functions in other cells and tissues (eg, smooth muscle cells and neural regulation of cardiac functions), highlighting a subject of future study.

## Clinical Relevance of Sorbs2 in Cardiac Disease

Precedent exists for various congenital cardiomyopathies to associate with Sorbs2 loss of function, including atrial septal defects and transposition of arteries,<sup>69,70</sup> which may be attributable to c-Abl/Notch/Shh signaling in cardiac stem cells.<sup>71</sup> Indeed, siRNA knockdown of Sorbs2 in cardiomyocyte differentiation studies decreases the expression of genes associated with cardiomyocyte maturation.<sup>72</sup> Although our work focuses on the slow progressing and adult onset of DCM, which likely results from subtle cytoskeletal changes/weakening, the possibility remains that subtle developmental alterations in Sorbs2-cKO mice could lead to slow progressing DCM.

Strong evidence supports that Sorbs2 is also associated with adult-onset heart disease; however, the clinical significance of this remains unknown. Our interrogation of independent RNA expression data and western blot data shows consistent upregulation in Sorbs2 across a range of myocardial diseases, as has been recently noted.<sup>73</sup> Furthermore, Sorbs2 protein is upregulated in LV noncompaction<sup>8</sup> and diabetic cardiomyopathy,<sup>6</sup> and is released from infarcted myocardium.<sup>4</sup> Upregulation is potentially mediated by Mef2 transcription factors,<sup>74</sup> although posttranscriptional regulation by disease-relevant microRNAs and RNA-binding proteins may also contribute.<sup>5,75,76</sup> For example, Sorbs2 mRNA harbors strong interaction sites for miR-29 and miR-30, which both show decreased abundances in failing hearts.<sup>77</sup> Although it remains unknown if and how these different components may contribute to overall Sorbs2 isoform expressions in heart, we speculate that Sorbs2 is upregulated in response to declining heart function, as cardiomyocytes attempt to increase the strength and stability of their cytoskeleton.

Beyond expression changes, our data queries also revealed several notable and relevant links between SORBS genetic variants and human phenotypes, including alterations in cardiac conduction and structure. Although some of these associations do not exceed genome-wide significance, cumulatively, these links

hint at the potential translational relevance of our mouse studies. Ultimately, more rigorous and targeted examinations in additional cohorts will be needed to clarify the potential clinical significance of these associations.

## Additional Future Directions

Looking beyond Sorbs2, we have not resolved if other SORBS proteins initially compensate, at least partially and/or temporarily, for the loss of Sorbs2 in cardiomyocytes to maintain cardiac function. Future work will need to expand investigations into the involvement of Sorbs1 and Sorbs3 in cardiac biology. Along with Sorbs2, both are expressed in myocyte and non-myocyte populations in the heart, show dysregulated expression in disease, and contain genetic variants associated with various cardiovascular phenotypes. Beyond this, protein structures are highly conserved among the 3 family members, and all localize along sarcomeres, at costameres, and at intercalated discs in heart tissues. SORBS family proteins can interact with one another, share several other protein interaction partners, and provide some redundancy in biological systems. However, each protein can also display independent properties related to mechanotransduction.<sup>78</sup> Considering that Sorbs1, Sorbs2, and Sorbs3 could collectively output at least 21 different protein isoforms, including several that are dysregulated in idiopathic or ischemic cardiomyopathy, it is clear that the known complexities of SORBS interactions and their contributions to cytoskeletal organization in cardiac biology and disease are only beginning to emerge.

## ARTICLE INFORMATION

Received February 14, 2022; accepted May 3, 2022.

### Affiliations

Department of Internal Medicine (J.M.M., X.Z., D.S.M., O.M.K., I.M.G., B.L., R.L.B.), Abboud Cardiovascular Research Center (J.M.M., X.Z., O.M.K., I.M.G., B.L., R.L.B.), and Department of Molecular Physiology and Biophysics (D.S.M.), University of Iowa Carver College of Medicine, Iowa City, IA; ; Department of Pharmacology and Systems Physiology (M.K., S.S.) and Division of Cardiovascular Health and Disease, Department of Internal Medicine, Heart, Lung, and Vascular Institute (M.K., S.S.), University of Cincinnati, OH.

### Acknowledgments

Dr Kenneth Margulies provided tissues through the Human Heart Tissue Bank at the University of Pennsylvania. Dr Chad Grueter provided  $\alpha$ -myosin heavy chain promoter driving Cre recombinase transgenic mice for use. Dr Benjamin Prosser provided detyrosinated and acetylated tubulin antibodies. Dr Robert Weiss, Kathy Zimmerman, and Alyssa Bosko contributed to mouse echocardiographic analyses. Dr Patrick Breheny advised on statistical analyses. Meg SmolikHagen contributed to mouse electrocardiographic analyses. Nathan Witmer and Gabrielle Abouassaly assisted with cloning and animal colony maintenance.

### Sources of Funding

Dr McLendon was supported by an American Heart Association fellowship 19POST34380640 and National Institutes of Health (NIH) fellowship T32-HL007121. Dr Matasic was supported by NIH fellowship F30-HL137272 and American Heart Association fellowship 17PRE33410450. Dr Kumar was supported by an American Heart Association fellowship 17PRE33630192.



Dr Grumbach has received support from NIH grants R01-HL108932, R01-EY031544, and R01-HL157956, and VA grant I01-BX000163. Dr Sadayappan has received support from NIH grants R01-AR078001, R01-HL130356, R01-HL105826, R38-HL155775, and R01-HL143490; American Heart Association grants 19UFEL34380251 and 19TPA34830084; the PLN Foundation (PLN crazy idea); and the Leducq Foundation (Transatlantic Network 18CVD01, PLN-CURE). Dr London has received research support from NIH grants R01-HL115955, R01-HL147545, and R01-HL152104. The University of Iowa Cardiovascular Phenotyping Core, directed by Dr Robert Weiss, is supported by NIH grants R01-HL142935 and 1S10OD019941. Dr Boudreau has received research support from NIH grants R01-HL144717, R01-HL148796, and R01-HL150557; American Heart Association 20IPA35360150.

## Disclosures

Dr Sadayappan provides consulting and collaborative research studies to the Leducq Foundation (CURE-PLAN), Red Saree Inc, Greater Cincinnati Tamil Sangam, AstraZeneca, MyoKardia, Merck, and Amgen, but such work is unrelated to the content of this article. The remaining authors have no disclosures to report.

## Supplemental Material

Tables S1–S5

Figures S1–S8

## REFERENCES

- Ntalla I, Weng L-C, Cartwright JH, Hall AW, Sveinbjornsson G, Tucker NR, Choi SH, Chaffin MD, Roselli C, Barnes MR, et al. Multi-ancestry GWAS of the electrocardiographic PR interval identifies 202 loci underlying cardiac conduction. *Nat Commun*. 2020;11:2542. doi: [10.1038/s41467-020-15706-x](https://doi.org/10.1038/s41467-020-15706-x)
- Carithers LJ, Ardlie K, Barcus M, Branton PA, Britton A, Buia SA, Compton CC, DeLuca DS, Peter-Demchok J, Gelfand ET, et al. A novel approach to high-quality postmortem tissue procurement: the GTEx project. *Biopreserv Biobank*. 2015;13:311–319. doi: [10.1089/bio.2015.0032](https://doi.org/10.1089/bio.2015.0032)
- Aguet F, Brown AA, Castel SE, Davis JR, He Y, Jo B, Mohammadi P, Park Y, Parsana P, Segrè AV, et al. Genetic effects on gene expression across human tissues. *Nature*. 2017;550:204–213. doi: [10.1038/nature24277](https://doi.org/10.1038/nature24277)
- Kakimoto Y, Ito S, Abiru H, Kotani H, Ozeki M, Tamaki K, Tsuruyama T. Sorbin and SH3 domain-containing protein 2 is released from infarcted heart in the very early phase: proteomic analysis of cardiac tissues from patients. *J Am Heart Assoc*. 2013;2:e000565. doi: [10.1161/jaha.113.000565](https://doi.org/10.1161/jaha.113.000565)
- Bang C, Batkai S, Dangwal S, Gupta SK, Foinquinos A, Holzmann A, Just A, Remke J, Zimmer K, Zeug A, et al. Cardiac fibroblast-derived microRNA passenger strand-enriched exosomes mediate cardiomyocyte hypertrophy. *J Clin Invest*. 2014;124:2136–2146. doi: [10.1172/jci70577](https://doi.org/10.1172/jci70577)
- Shao M, Chen J, Zheng S. Comparative proteomics analysis of myocardium in mouse model of diabetic cardiomyopathy using the iTRAQ technique. *Adv Clin Exp Med*. 2018;27:1469–1475. doi: [10.17219/acem/74539](https://doi.org/10.17219/acem/74539)
- Ding Y, Yang J, Chen P, Lu T, Jiao K, Tester DJ, Giudicessi JR, Jiang K, Ackerman MJ, Li Y, et al. Knockout of SORBS2 protein disrupts the structural integrity of intercalated disc and manifests features of arrhythmogenic cardiomyopathy. *J Am Heart Assoc*. 2020;9:e017055. doi: [10.1161/jaha.119.017055](https://doi.org/10.1161/jaha.119.017055)
- Li C, Liu F, Liu S, Pan H, Du H, Huang J, Xie Y, Li Y, Zhao R, Wei Y. Elevated myocardial SORBS2 and the underlying implications in left ventricular noncompaction cardiomyopathy. *EBioMedicine*. 2020;53:102695. doi: [10.1016/j.ebiom.2020.102695](https://doi.org/10.1016/j.ebiom.2020.102695)
- Zhang Q, Gao X, Li C, Feliciano C, Wang D, Zhou D, Mei Y, Monteiro P, Anand M, Itohara S, et al. Impaired dendritic development and memory in Sorbs2 knock-out mice. *J Neurosci*. 2016;36:2247–2260. doi: [10.1523/jneurosci.2528-15.2016](https://doi.org/10.1523/jneurosci.2528-15.2016)
- Agah R, Frenkel PA, French BA, Michael LH, Overbeek PA, Schneider MD. Gene recombination in postmitotic cells. Targeted expression of Cre recombinase provokes cardiac-restricted, site-specific rearrangement in adult ventricular muscle in vivo. *J Clin Invest*. 1997;100:169–179. doi: [10.1172/jci119509](https://doi.org/10.1172/jci119509)
- Spitler KM, Ponce JM, Oudit GY, Hall DD, Grueter CE. Cardiac Med1 deletion promotes early lethality, cardiac remodeling, and transcriptional reprogramming. *Am J Physiol Heart Circ Physiol*. 2017;312:H768–H780. doi: [10.1152/ajpheart.00728.2016](https://doi.org/10.1152/ajpheart.00728.2016)
- Hu P, Zhang D, Swenson L, Chakrabarti G, Abel ED, Litwin SE. Minimally invasive aortic banding in mice: effects of altered cardiomyocyte insulin signaling during pressure overload. *Am J Physiol Heart Circ Physiol*. 2003;285:H1261–H1269. doi: [10.1152/ajpheart.00108.2003](https://doi.org/10.1152/ajpheart.00108.2003)
- Calligaris SD, Ricca M, Conget P. Cardiac stress test induced by dobutamine and monitored by cardiac catheterization in mice. *J Vis Exp*. 2013;50050. doi: [10.3791/50050](https://doi.org/10.3791/50050)
- Lynch TL, Kumar M, McNamara JW, Kuster DWD, Sivaguru M, Singh RR, Previs MJ, Lee KH, Kuffel G, Zilliox MJ, et al. Amino terminus of cardiac myosin binding protein-C regulates cardiac contractility. *J Mol Cell Cardiol*. 2021;156:33–44. doi: [10.1016/j.yjmcc.2021.03.009](https://doi.org/10.1016/j.yjmcc.2021.03.009)
- Golden H, Gollapudi D, Gerilechaogetu F, Li J, Cristales R, Peng X, Dostal D. Isolation of cardiac myocytes and fibroblasts from neonatal rat pups. *Methods Mol Biol*. 2012;843:205–214. doi: [10.1007/978-1-61779-523-7\\_20](https://doi.org/10.1007/978-1-61779-523-7_20)
- Matašić DS, Yoon J-Y, McLendon JM, Mehdi H, Schmidt MS, Greiner AM, Quinones P, Morgan GM, Boudreau RL, Irani K, et al. Modulation of the cardiac sodium channel Na(V)1.5 peak and late currents by NAD(+) precursors. *J Mol Cell Cardiol*. 2020;141:70–81. doi: [10.1016/j.yjmcc.2020.01.013](https://doi.org/10.1016/j.yjmcc.2020.01.013)
- van Heesch S, Witte F, Schneider-Lunitz V, Schulz JF, Adami E, Faber AB, Kirchner M, Maatz H, Blachut S, Sandmann C-L, et al. The translational landscape of the human heart. *Cell*. 2019;178:242–260.e229. doi: [10.1016/j.cell.2019.05.010](https://doi.org/10.1016/j.cell.2019.05.010)
- Sweet ME, Cociolo A, Slavov D, Jones KL, Sweet JR, Graw SL, Reece TB, Ambardekar AV, Bristow MR, Mestroni L, et al. Transcriptome analysis of human heart failure reveals dysregulated cell adhesion in dilated cardiomyopathy and activated immune pathways in ischemic heart failure. *BMC Genom*. 2018;19:812. doi: [10.1186/s12864-018-5213-9](https://doi.org/10.1186/s12864-018-5213-9)
- Doroudgar S, Hofmann C, Boileau E, Malone B, Riechert E, Gorska AA, Jakobi T, Sandmann C, Jürgensen L, Kmietczyk V, et al. Monitoring cell-type-specific gene expression using ribosome profiling in vivo during cardiac hemodynamic stress. *Circ Res*. 2019;125:431–448. doi: [10.1161/CIRCRESAHA.119.314817](https://doi.org/10.1161/CIRCRESAHA.119.314817)
- Buniello A, MacArthur JAL, Cerezo M, Harris LW, Hayhurst J, Mangano C, McMahon A, Morales J, Mountjoy E, Sollis E, et al. The NHGRI-EBI GWAS Catalog of published genome-wide association studies, targeted arrays and summary statistics 2019. *Nucleic Acids Res*. 2019;47:D1005–D1012. doi: [10.1093/nar/gky1120](https://doi.org/10.1093/nar/gky1120)
- Christophersen IE, Magnani JW, Yin X, Barnard J, Weng L-C, Arking DE, Niemeijer MN, Lubitz SA, Avery CL, Duan Q, et al. Fifteen genetic loci associated with the electrocardiographic P wave. *Circ Cardiovasc Genet*. 2017;10:e001667. doi: [10.1161/circgenetics.116.001667](https://doi.org/10.1161/circgenetics.116.001667)
- Esslinger U, Garnier S, Korniat A, Proust C, Kararigas G, Müller-Nurasyid M, Empana J-P, Morley MP, Perret C, Stark K, et al. Exome-wide association study reveals novel susceptibility genes to sporadic dilated cardiomyopathy. *PLoS One*. 2017;12:e0172995. doi: [10.1371/journal.pone.0172995](https://doi.org/10.1371/journal.pone.0172995)
- Welsh P, Preiss D, Hayward C, Shah ASV, McAllister D, Briggs A, Boachie C, McConnachie A, Padmanabhan S, Welsh C, et al. Cardiac troponin T and troponin I in the general population. *Circulation*. 2019;139:2754–2764. doi: [10.1161/circulationaha.118.038529](https://doi.org/10.1161/circulationaha.118.038529)
- Agliano Taliun SA, VandeHaar P, Boughton AP, Welch RP, Taliun D, Schmidt EM, Zhou W, Nielsen JB, Willer CJ, Lee S, et al. Exploring and visualizing large-scale genetic associations by using PheWeb. *Nat Genet*. 2020;52:550–552. doi: [10.1038/s41588-020-0622-5](https://doi.org/10.1038/s41588-020-0622-5)
- Murray SS, Smith EN, Villarasa N, Nahey T, Lande J, Goldberg H, Shaw M, Rosenthal L, Ramza B, Alaeddini J, et al. Genome-wide association of implantable cardioverter-defibrillator activation with life-threatening arrhythmias. *PLoS One*. 2012;7:e25387. doi: [10.1371/journal.pone.0025387](https://doi.org/10.1371/journal.pone.0025387)
- van Setten J, Brody JA, Jamshidi Y, Swenson BR, Butler AM, Campbell H, Del Greco FM, Evans DS, Gibson Q, Gudbjartsson DF, et al. PR interval genome-wide association meta-analysis identifies 50 loci associated with atrial and atrioventricular electrical activity. *Nat Commun*. 2018;9:2904. doi: [10.1038/s41467-018-04766-9](https://doi.org/10.1038/s41467-018-04766-9)
- Ashar FN, Mitchell RN, Albert CM, Newton-Cheh C, Brody JA, Müller-Nurasyid M, Moes A, Meitinger T, Mak A, Huikuri H, et al. A comprehensive evaluation of the genetic architecture of sudden cardiac arrest. *Eur Heart J*. 2018;39:3961–3969. doi: [10.1093/eurheartj/ehy474](https://doi.org/10.1093/eurheartj/ehy474)

28. Kichaev G, Bhatia G, Loh PR, Gazal S, Burch K, Freund MK, Schoech A, Pasaniuc B, Price AL. Leveraging polygenic functional enrichment to improve GWAS power. *Am J Hum Genet.* 2019;104:65–75. doi: [10.1016/j.ajhg.2018.11.008](https://doi.org/10.1016/j.ajhg.2018.11.008)
29. Qian LL, Sun X, Yang J, Wang XL, Ackerman MJ, Wang RX, Xu X, Lee HC, Lu T. Changes in ion channel expression and function associated with cardiac arrhythmogenic remodeling by Sorbs2. *Biochim Biophys Acta Mol Basis Dis.* 2021;1867:166247. doi: [10.1016/j.bbadis.2021.166247](https://doi.org/10.1016/j.bbadis.2021.166247)
30. Pugach EK, Richmond PA, Azofeifa JG, Dowell RD, Leinwand LA. Prolonged Cre expression driven by the  $\alpha$ -myosin heavy chain promoter can be cardiotoxic. *J Mol Cell Cardiol.* 2015;86:54–61. doi: [10.1016/j.yjmcc.2015.06.019](https://doi.org/10.1016/j.yjmcc.2015.06.019)
31. Waggoner AD, Adyanthaya AV, Quinones MA, Alexander JK. Left atrial enlargement. Echocardiographic assessment of electrocardiographic criteria. *Circulation.* 1976;54:553–557. doi: [10.1161/01.cir.54.4.553](https://doi.org/10.1161/01.cir.54.4.553)
32. Ruan Y, Liu N, Priori SG. Sodium channel mutations and arrhythmias. *Nat Rev Cardiol.* 2009;6:337–348. doi: [10.1038/nrcardio.2009.44](https://doi.org/10.1038/nrcardio.2009.44)
33. Kioka N, Ueda K, Amachi T. Vinexin, CAP/ponsin, ArgBP2: a novel adaptor protein family regulating cytoskeletal organization and signal transduction. *Cell Struct Funct.* 2002;27:1–7. doi: [10.1247/csf.27.1](https://doi.org/10.1247/csf.27.1)
34. Hallock PT, Chin S, Blais S, Neubert TA, Glass DJ. Sorbs1 and -2 interact with CrkL and are required for acetylcholine receptor cluster formation. *Mol Cell Biol.* 2016;36:262–270. doi: [10.1128/mcb.00775-15](https://doi.org/10.1128/mcb.00775-15)
35. Pleger ST, Shan C, Ksienzyk J, Bekeredjian R, Boekstegers P, Hinkel R, Schinkel S, Leuchs B, Ludwig J, Qiu G, et al. Cardiac AAV9-S100A1 gene therapy rescues post-ischemic heart failure in a preclinical large animal model. *Sci Transl Med.* 2011;3:92ra64. doi: [10.1126/scitranslmed.3002097](https://doi.org/10.1126/scitranslmed.3002097)
36. Most P, Remppis A, Pleger ST, Katus HA, Koch WJ. S100A1: a novel inotropic regulator of cardiac performance. Transition from molecular physiology to pathophysiological relevance. *Am J Physiol Regul Integr Comp Physiol.* 2007;293:R568–R577. doi: [10.1152/ajpregu.00075.2007](https://doi.org/10.1152/ajpregu.00075.2007)
37. Li C, Zheng Y, Liu Y, Jin GH, Pan H, Yin F, Wu J. The interaction protein of SORBS2 in myocardial tissue to find out the pathogenic mechanism of LVNC disease. *Aging (Albany NY).* 2022;14:800–810. doi: [10.18632/aging.203841](https://doi.org/10.18632/aging.203841)
38. Fredriksson-Lidman K, Van Itallie CM, Tietgens AJ, Anderson JM. Sorbin and SH3 domain-containing protein 2 (SORBS2) is a component of the acto-myosin ring at the apical junctional complex in epithelial cells. *PLoS One.* 2017;12:e0185448. doi: [10.1371/journal.pone.0185448](https://doi.org/10.1371/journal.pone.0185448)
39. Li L, Zhang Q, Zhang X, Zhang J, Wang X, Ren J, Jia J, Zhang D, Jiang X, Zhang J, et al. Microtubule associated protein 4 phosphorylation leads to pathological cardiac remodeling in mice. *EBioMedicine.* 2018;37:221–235. doi: [10.1016/j.ebiom.2018.10.017](https://doi.org/10.1016/j.ebiom.2018.10.017)
40. Yashirogi S, Nagao T, Nishida Y, Takahashi Y, Qaqorh T, Yazawa I, Katayama T, Kioka H, Matsui TS, Saito S, et al. AMPK regulates cell shape of cardiomyocytes by modulating turnover of microtubules through CLIP-170. *EMBO Rep.* 2021;22:e50949. doi: [10.15252/embr.202050949](https://doi.org/10.15252/embr.202050949)
41. Chen CY, Caporizzo MA, Bedi K, Vite A, Bogush AI, Robison P, Heffler JG, Salomon AK, Kelly NA, Babu A, et al. Suppression of detyrosinated microtubules improves cardiomyocyte function in human heart failure. *Nat Med.* 2018;24:1225–1233. doi: [10.1038/s41591-018-0046-2](https://doi.org/10.1038/s41591-018-0046-2)
42. Schuldt M, Pei J, Harakalova M, Dorsch LM, Schlossarek S, Mokry M, Knol JC, Pham TV, Schellhorst T, Piersma SR, et al. Proteomic and functional studies reveal detyrosinated tubulin as treatment target in sarcomere mutation-induced hypertrophic cardiomyopathy. *Circ Heart Fail.* 2021;14:e007022. doi: [10.1161/circheartfailure.120.007022](https://doi.org/10.1161/circheartfailure.120.007022)
43. Belmadani S, Poüs C, Ventura-Clapier R, Fischmeister R, Méry PF. Post-translational modifications of cardiac tubulin during chronic heart failure in the rat. *Mol Cell Biochem.* 2002;237:39–46. doi: [10.1023/a:1016554104209](https://doi.org/10.1023/a:1016554104209)
44. Sato H, Nagai T, Kuppuswamy D, Narishige T, Koide M, Menick DR, Cooper G IV. Microtubule stabilization in pressure overload cardiac hypertrophy. *J Cell Biol.* 1997;139:963–973. doi: [10.1083/jcb.139.4.963](https://doi.org/10.1083/jcb.139.4.963)
45. Nishimura S, Nagai S, Katoh M, Yamashita H, Saeki Y, Okada J, Hisada T, Nagai R, Sugiura S. Microtubules modulate the stiffness of cardiomyocytes against shear stress. *Circ Res.* 2006;98:81–87. doi: [10.1161/01.RES.0000197785.51819.e8](https://doi.org/10.1161/01.RES.0000197785.51819.e8)
46. Swiatlowska P, Sanchez-Alonso JL, Wright PT, Novak P, Gorelik J. Microtubules regulate cardiomyocyte transversal Young's modulus. *Proc Natl Acad Sci USA.* 2020;117:2764–2766. doi: [10.1073/pnas.1917171117](https://doi.org/10.1073/pnas.1917171117)
47. Robison P, Caporizzo MA, Ahmadzadeh H, Bogush AI, Chen CY, Margulies KB, Shenoy VB, Prosser BL. Detyrosinated microtubules buckle and bear load in contracting cardiomyocytes. *Science.* 2016;352:aaf0659. doi: [10.1126/science.aaf0659](https://doi.org/10.1126/science.aaf0659)
48. Caporizzo MA, Chen CY, Bedi K, Margulies KB, Prosser BL. Microtubules increase diastolic stiffness in failing human cardiomyocytes and myocardium. *Circulation.* 2020;141:902–915. doi: [10.1161/circulationaha.119.043930](https://doi.org/10.1161/circulationaha.119.043930)
49. Grimes KM, Prasad V, McNamara JW. Supporting the heart: functions of the cardiomyocyte's non-sarcomeric cytoskeleton. *J Mol Cell Cardiol.* 2019;131:187–196. doi: [10.1016/j.yjmcc.2019.04.002](https://doi.org/10.1016/j.yjmcc.2019.04.002)
50. Wang B, Golemis EA, Kruh GD. ArgBP2, a multiple Src homology 3 domain-containing, Arg/Abl-interacting protein, is phosphorylated in v-Abl-transformed cells and localized in stress fibers and cardiocyte Z-disks. *J Biol Chem.* 1997;272:17542–17550. doi: [10.1074/jbc.272.28.17542](https://doi.org/10.1074/jbc.272.28.17542)
51. Luck K, Kim D-K, Lambourne L, Spirohn K, Begg BE, Bian W, Brignall R, Cafarelli T, Campos-Laborie FJ, Charlotiaux B, et al. A reference map of the human binary protein interactome. *Nature.* 2020;580:402–408. doi: [10.1038/s41586-020-2188-x](https://doi.org/10.1038/s41586-020-2188-x)
52. Soubeyran P, Barac A, Szymkiewicz I, Dikic I. Cbl-ArgBP2 complex mediates ubiquitination and degradation of c-Abl. *Biochem J.* 2003;370:29–34. doi: [10.1042/bj20021539](https://doi.org/10.1042/bj20021539)
53. Cestra G, Toomre D, Chang S, De Camilli P. The Abl/Arg substrate ArgBP2/nArgBP2 coordinates the function of multiple regulatory mechanisms converging on the actin cytoskeleton. *Proc Natl Acad Sci USA.* 2005;102:1731–1736. doi: [10.1073/pnas.0409376102](https://doi.org/10.1073/pnas.0409376102)
54. Qiu Z, Cang Y, Goff SP. c-Abl tyrosine kinase regulates cardiac growth and development. *Proc Natl Acad Sci USA.* 2010;107:1136–1141. doi: [10.1073/pnas.0913131107](https://doi.org/10.1073/pnas.0913131107)
55. Zandy NL, Playford M, Pendergast AM. Abl tyrosine kinases regulate cell-cell adhesion through Rho GTPases. *Proc Natl Acad Sci USA.* 2007;104:17686–17691. doi: [10.1073/pnas.0703077104](https://doi.org/10.1073/pnas.0703077104)
56. Miller AL, Wang Y, Mooseker MS, Koleske AJ. The Abl-related gene (Arg) requires its F-actin-microtubule cross-linking activity to regulate lamellipodial dynamics during fibroblast adhesion. *J Cell Biol.* 2004;165:407–419. doi: [10.1083/jcb.200308055](https://doi.org/10.1083/jcb.200308055)
57. Colicelli J. ABL tyrosine kinases: evolution of function, regulation, and specificity. *Sci Signal.* 2010;3:re6. doi: [10.1126/scisignal.3139re6](https://doi.org/10.1126/scisignal.3139re6)
58. Wang Y, Miller AL, Mooseker MS, Koleske AJ. The Abl-related gene (Arg) nonreceptor tyrosine kinase uses two F-actin-binding domains to bundle F-actin. *Proc Natl Acad Sci USA.* 2001;98:14865–14870. doi: [10.1073/pnas.251249298](https://doi.org/10.1073/pnas.251249298)
59. Hu Y, Lyu W, Lowery LA, Koleske AJ. Regulation of MT dynamics via direct binding of an Abl family kinase. *J Cell Biol.* 2019;218:3986–3997. doi: [10.1083/jcb.201812144](https://doi.org/10.1083/jcb.201812144)
60. Haglund K, Ivankovic-Dikic I, Shimokawa N, Kruh GD, Dikic I. Recruitment of Pyk2 and Cbl to lipid rafts mediates signals important for actin reorganization in growing neurites. *J Cell Sci.* 2004;117:2557–2568. doi: [10.1242/jcs.01148](https://doi.org/10.1242/jcs.01148)
61. Teckchandani AM, Birukova AA, Tar K, Verin AD, Tsygankov AY. The multidomain protooncogenic protein c-Cbl binds to tubulin and stabilizes microtubules. *Exp Cell Res.* 2005;306:114–127. doi: [10.1016/j.yexcr.2005.02.014](https://doi.org/10.1016/j.yexcr.2005.02.014)
62. Hein M, Hubner N, Poser I, Cox J, Nagaraj N, Toyoda Y, Gak I, Weisswange I, Mansfeld J, Buchholz F, et al. A human interactome in three quantitative dimensions organized by stoichiometries and abundances. *Cell.* 2015;163:712–723. doi: [10.1016/j.cell.2015.09.053](https://doi.org/10.1016/j.cell.2015.09.053)
63. Sweet ES, Previtera ML, Fernández JR, Charych EI, Tseng C-Y, Kwon M, Starovoytov V, Zheng JQ, Firestein BL. PSD-95 alters microtubule dynamics via an association with EB3. *J Neurosci.* 2011;31:1038. doi: [10.1523/JNEUROSCI.1205-10.2011](https://doi.org/10.1523/JNEUROSCI.1205-10.2011)
64. Glazier AA, Hafeez N, Mellacheruvu D, Basrur V, Nesvizhskii AI, Lee LM, Shao H, Tang VI, Yob JM, Gestwicki JE, et al. HSC70 is a chaperone for wild-type and mutant cardiac myosin binding protein C. *JCI Insight.* 2018;3:e99319. doi: [10.1172/jci.insight.99319](https://doi.org/10.1172/jci.insight.99319)
65. Sanger JM, Wang J, Gleason LM, Chowrashi P, Dube DK, Mittal B, Zhukareva V, Sanger JW. Arg/Abl-binding protein, a Z-body and Z-band protein, binds sarcomeric, costameric, and signaling molecules. *Cytoskeleton (Hoboken).* 2010;67:808–823. doi: [10.1002/cm.20490](https://doi.org/10.1002/cm.20490)
66. Asimaki A, Tandri H, Huang H, Halushka MK, Gautam S, Basso C, Thiene G, Tsatsopoulou A, Protonotarios N, McKenna WJ, et al. A new diagnostic test for arrhythmogenic right ventricular cardiomyopathy. *N Engl J Med.* 2009;360:1075–1084. doi: [10.1056/NEJMoa0808138](https://doi.org/10.1056/NEJMoa0808138)
67. Zhao L, Wang W, Huang S, Yang Z, Xu L, Yang Q, Zhou X, Wang J, Shen Q, Wang C, et al. The RNA binding protein SORBS2 suppresses

- metastatic colonization of ovarian cancer by stabilizing tumor-suppressive immunomodulatory transcripts. *Genome Biol.* 2018;19:35. doi: [10.1186/s13059-018-1412-6](https://doi.org/10.1186/s13059-018-1412-6)
68. Lv Q, Dong F, Zhou Y, Cai Z, Wang G. RNA-binding protein SORBS2 suppresses clear cell renal cell carcinoma metastasis by enhancing MTUS1 mRNA stability. *Cell Death Dis.* 2020;11:1056. doi: [10.1038/s41419-020-03268-1](https://doi.org/10.1038/s41419-020-03268-1)
69. Maurin ML, Labrune P, Brisset S, Le Lorc'h M, Pineau D, Castel C, Romana S, Tachdjian G. Molecular cytogenetic characterization of a 4p15.1-pter duplication and a 4q35.1-qter deletion in a recombinant of chromosome 4 pericentric inversion. *Am J Med Genet A.* 2009;149A:226–231. doi: [10.1002/ajmg.a.32603](https://doi.org/10.1002/ajmg.a.32603)
70. Molck MC, Simioni M, Paiva Vieira T, Sgardiolli IC, Paoli Monteiro F, Souza J, Fett-Conte AC, Félix TM, Lopes Monlléo I, Gil-da-Silva-Lopes VL. Genomic imbalances in syndromic congenital heart disease. *J Pediatr (Rio J).* 2017;93:497–507. doi: [10.1016/j.jpmed.2016.11.007](https://doi.org/10.1016/j.jpmed.2016.11.007)
71. Liang F, Wang BO, Geng J, You G, Fa J, Zhang M, Sun H, Chen H, Fu Q, Zhang X, et al. SORBS2 is a genetic factor contributing to cardiac malformation of 4q deletion syndrome patients. *Elife.* 2021;10:e67481. doi: [10.7554/eLife.67481](https://doi.org/10.7554/eLife.67481)
72. Fu K, Nakano H, Morselli M, Chen T, Pappoe H, Nakano A, Pellegrini M. A temporal transcriptome and methylome in human embryonic stem cell-derived cardiomyocytes identifies novel regulators of early cardiac development. *Epigenetics.* 2018;13:1013–1026. doi: [10.1080/1559294.2018.1526029](https://doi.org/10.1080/1559294.2018.1526029)
73. Vigil-Garcia M, Demkes CJ, Eding JEC, Versteeg D, de Ruiter H, Perini I, Kooijman L, Gladka MM, Asselbergs FW, Vink A, et al. Gene expression profiling of hypertrophic cardiomyocytes identifies new players in pathological remodelling. *Cardiovasc Res.* 2021;117:1532–1545. doi: [10.1093/cvr/cvaa233](https://doi.org/10.1093/cvr/cvaa233)
74. Wales S, Hashemi S, Blais A, McDermott JC. Global MEF2 target gene analysis in cardiac and skeletal muscle reveals novel regulation of DUSP6 by p38MAPK-MEF2 signaling. *Nucleic Acids Res.* 2014;42:11349–11362. doi: [10.1093/nar/gku813](https://doi.org/10.1093/nar/gku813)
75. Dixon DM, Choi J, El-Ghazali A, Park SY, Roos KP, Jordan MC, Fishbein MC, Comai L, Reddy S. Loss of muscleblind-like 1 results in cardiac pathology and persistence of embryonic splice isoforms. *Sci Rep.* 2015;5:9042. doi: [10.1038/srep09042](https://doi.org/10.1038/srep09042)
76. Wang H, Bei Y, Shen S, Huang P, Shi J, Zhang J, Sun QI, Chen Y, Yang Y, Xu T, et al. miR-21-3p controls sepsis-associated cardiac dysfunction via regulating SORBS2. *J Mol Cell Cardiol.* 2016;94:43–53. doi: [10.1016/j.yjmcc.2016.03.014](https://doi.org/10.1016/j.yjmcc.2016.03.014)
77. Spengler RM, Zhang X, Cheng C, McLendon JM, Skeie JM, Johnson FL, Davidson BL, Boudreau RL. Elucidation of transcriptome-wide microRNA binding sites in human cardiac tissues by Ago2 HITS-CLIP. *Nucleic Acids Res.* 2016;44:7120–7131. doi: [10.1093/nar/gkw640](https://doi.org/10.1093/nar/gkw640)
78. Ichikawa T, Kita M, Matsui TS, Nagasato AI, Araki T, Chiang S-H, Sezaki T, Kimura Y, Ueda K, Deguchi S, et al. Vinexin family (SORBS) proteins play different roles in stiffness-sensing and contractile force generation. *J Cell Sci.* 2017;130:3517–3531. doi: [10.1242/jcs.200691](https://doi.org/10.1242/jcs.200691)

# **SUPPLEMENTAL MATERIAL**



**Table S1. Supplement to Materials and Methods.**

**Table includes buffer recipes, antibodies for western blot, antibodies for immunofluorescence microscopy, and primer sequences.**

<b>Method</b>	<b>Solution</b>	<b>Composition</b>
Myofiber Mechanics	pCa 9.0 Relaxing Buffer	in mM: 7 EGTA, 100 BES, 0.017 CaCl <sub>2</sub> , 5.491 MgCl <sub>2</sub> , 5 DTT, 15 creatine phosphate, and 4.655 ATP; pH adjusted to 7.0 with KOH and ionic strength set to 180 with K-propionate
Myofiber Mechanics	pCa4.5 Activating Buffer	in mM: 7 EGTA, 100 BES, 7.005 CaCl <sub>2</sub> , 5.294 MgCl <sub>2</sub> , 5 DTT, 15 creatine phosphate, and 4.724 ATP; pH adjusted to 7.0 with KOH and ionic strength set to 180 with K-propionate
Western Blot	Tissue Lysis Buffer	in mM: 50 Tris, 150 NaCl, 10 NaF, 5 EGTA, 5 EDTA, 10 NaF, 1 PMSF, 1 sodium orthovanadate, 12 sodium deoxycholate, with 0.5% (w/v) Triton X-100, 1% (w/v) SDS, and protease inhibitor (Roche, 11873580001)
Western Blot	Blocking Buffer	in mM: 20 Tris, 500 NaCl, 0.05% (v/v) Tween-20, with 5% (w/v) nonfat dry milk
Microtubule Assay	Microtubule Stabilization Buffer	in mM: 25 Na <sub>4</sub> P <sub>2</sub> O <sub>7</sub> , 10 Na <sub>2</sub> HPO <sub>4</sub> , 0.5 EGTA, 0.5 MgSO <sub>4</sub> , 0.5 GTP, 1.0 ATP, and with (% v/v), 50% glycerol, 5% DMSO, 1% NP40 alternative (Millipore, 492018), and with protease/phosphatase inhibitor (Pierce, A32961)
Immunofluorescence	Permeabilization buffer	in mM: 20 Tris, 500 NaCl, with 0.2% v/v TritonX-100
Immunofluorescence	Blocking buffer	in mM: 20 Tris, 500 NaCl, with 0.02% (v/v) TritonX-100, 2% (w/v) BSA, and 10% (v/v) goat serum

Electrophysiology	Internal Solution	in mM: 10 NaCl, 90 aspartic acid, 70 CsOH, 10 EGTA, 20 CsCl, 10 HEPES, and pH adjusted to 7.35 using CsOH
Electrophysiology	Extracellular Solution	in mM: 145 NaCl, 4.5 KCl, 10 HEPES, 1 MgCl <sub>2</sub> , 1.5 CaCl <sub>2</sub> , and pH adjusted to 7.35 using CsOH
Cell Culture	Cardiomyocyte Media	DMEM/F12 media supplemented with 5% horse serum, 10 mM HEPES, 1% ITS, 15 µg/mL Gentamycin, and 100 µM BRDU

## Antibodies for Western Blot

Antibody	Source	Product #	Dilution Ratio
acetyl-TUBA	Cell Signaling	12152S	1:1000
ACTN2	Sigma	A7732	1:1000
ATP2A2	Thermo	2a7-a1	1:1000
CDH2	BD Transduction Labs	610920	1:1000
CTNNB1	Sigma	PLA0230	1:2000
DES	DSHB	D3	1:50
dTyr-TUBA	Abcam	ab48389	1:1000
GAPDH	Santa Cruz	sc-25778	1:3000
GJA1	Cell Signaling	3512	1:500
GJA1	Abclonal	A11752	1:1000
GJA5	Abclonal	A11752	1:500
ITGB1D	Abcam	ab8991	1:500
JPH2	Santa Cruz	sc-51313	1:2000

JUP	Proteintech	11146-1-AP	1:1000
KCNH2	Alomone	APC-062	1:500
MAPRE1	Sigma	e3406	1:1000
MAPRE1	BD Transduction Labs	610535	1:1000
MLC1	DSHB	f310	1:500
MYBPC3	S. Sadayappan, PMID# 19237661	custom	1:1000
p282-MYBPC3	S. Sadayappan, PMID# 19237661	custom	1:1000
S100A1	Proteintech	16027-1-AP	1:500
SCN5A	Alomone	493-511	1:500
SORBS1	Aviva	ARP51833_P050	1:500
SORBS2	Proteintech	24643-1-AP	1:1000
SORBS2	Sigma	SAB4200183	1:1000
TJP1	Proteintech	21773-1-AP	1:500
p22/23-TNNI3	Sigma	sab4504001	1:1000
TNNI3	Sigma	WH0007137M4	1:1000
TPM1	DSHB	CH1	1:50
TUBA	Cell Signaling	3873S	1:1000
TUBB	DSHB	E7	1:500
VCL	Cell Signaling	13901	1:1000
anti-mouse-HRP	Jackson Immunoresearch	115-035-146	1:25,000
anti-rabbit-HRP	Jackson Immunoresearch	111-035-144	1:25,000
anti-mouse-DyLight-680	Invitrogen	35519	1:5000
anti-rabbit-DyLight-800	Invitrogen	sa5-10036	1:5000

## Antibodies for Immunofluorescent Microscopy

Antibody	Source	Product #	Dilution/final concentration
ACTN2	sigma	A7732	1:1000
ACTN2	Sigma	A7732	1:1000
GJA1	Abclonal	A11752	1:100
SORBS2	Proteintech	24643-1-AP	1:500
SORBS2	Sigma	SAB4200183	1:500
VCL	Cell Signaling	13901	1:500
WGA-af488	Thermo Fisher Sci./Invitrogen/Life Techn.	W11261	10 ug/mL
Phalloidin- af568	Thermo Fisher Sci./Invitrogen/Life Techn.	A12380	~ 66 nM
anti-mouse- 488	Thermo Fisher Sci./Invitrogen/Life Techn.	A11017	1:1000
anti-mouse- 568	Thermo Fisher Sci./Invitrogen/Life Techn.	A11019	1:1000
anti-mouse- 647	Thermo Fisher Sci./Invitrogen/Life Techn.	A21237	1:1000
anti-rabbit-488	Thermo Fisher Sci./Invitrogen/Life Techn.	A11070	1:1000
anti-rabbit-568	Thermo Fisher Sci./Invitrogen/Life Techn.	A21069	1:1000
anti-rabbit-647	Thermo Fisher Sci./Invitrogen/Life Techn.	A21246	1:1000
anti-rat-488	Thermo Fisher Sci./Invitrogen/Life Techn.	A11006	1:1000



anti-rat-568	Thermo Fisher Sci./Invitrogen/Life Techn.	A11077	1:1000
--------------	---	--------	--------

### Primers Sequences Listed 5' to 3'

Reson	Primer	Sequence
Genotyping	SORBS2gtF1	GCAGCCATCGTCATGCTTGTG
Genotyping	SORBS2gtF2	CACCTTAGGTTCTAGGGATCGAGCTC
Genotyping	aMHCgtF1	CTAGCCCACACCAGAAATGACAGAC
Genotyping	CREgtR1	GAACCTCATCACTCGTTGCATCGAC
cloning	mmSORBS2F	AAAAAACGCGTAGCCATGAATACAGATAGCGGTGGGTGT GCTCGCAAAC
cloning	mmSORBS2R	AAAAAGCTAGCAGGTGAGTCACAGCCTTTTGACATAG

**Table S2. Dataset description for Sorbs2 RNA dysregulation in heart failure.**

Table includes description for datasets used in Figure 1a. Information includes the accession number (Acc#), disease, sample number for control and disease groups, log2-fold-change value (l2fc) and -log10 p-value (-l10P). Blank rows correspond to the gaps in the Figure 1a plot.

Acc#	Disease	Control N	Disease N	l2fc	-l10P
GSE36961	HCM	39	106	0.827	31.157
GSE29819	ARVC	6	6	0.466	3.623
GSE57345	Idiopathic	139	84	0.414	26.111
EGAS00001002454	DCM	113	149	0.290	25.738
GSE3586	DCM	15	13	1.009	7.438
GSE5406	Idiopathic	16	86	0.677	5.300
GSE1145	Idiopathic	11	15	1.454	5.126
GSE79962	HF	11	9	0.416	3.876
GSE46224	HF	8	8	0.650	2.988
GSE53081	Idiopathic	4	8	0.362	1.166
GSE57345	Ischemic	139	96	0.254	6.767
GSE1145	Ischemic	11	11	1.595	3.699
GSE5406	Ischemic	16	108	0.463	2.062
GSE53081	Ischemic	4	8	0.533	2.023
GSE16499	Ischemic	15	15	0.264	0.903
GSE48166	Ischemic	15	15	0.372	0.210
GSE13874	genetic HF	4	4	1.565	5.903
GSE68518	genetic HF	6	6	0.554	4.559
GSE36074	TAC/HF (decompensated)	5	7	0.596	5.712
GSE58455	TAC	4	4	0.557	4.413
GSE36074	TAC/NF (compensated)	5	7	0.368	3.285
GSE4648	MI	10	12	0.884	2.526
GSE107569	TAC	6	6	0.786	2.151
GSE35350	TAC	4	3	0.670	2.025
GSE5500	TAC	4	6	0.384	1.290
GSE5996	cells Strech	2	2	0.602	5.648
GSE5996	cells PE	2	2	0.587	3.358
GSE73896	cells-PE	4	4	0.524	2.770



Table S4. Mice heart failure model phenotyping data.

Table describes phenotyping data (grouping, gravimetric, and echocardiographic measurements) of control and mouse heart failure samples used in Figure

1c. Group averages and statistical significance (two sided T-test) between groups is presented, (p < 0.05 is highlighted red). C57BL6J

Sham vs miTAC Data

Description / Measurement	Sham					miTAC					Avg-Sham	Avg-TAC	p value (ttest)		
	1 NA	2	3	4 NA	5	6 NA	7								
Used in Western Lane Number	1	2	3	4	5	6	7	8	9	10	11	12			
Group	SHAM	SHAM	SHAM	SHAM	TAC(38g)	TAC(38g)	TAC(38g)	TAC(38g)	TAC(38g)	TAC(38g)	TAC(38g)				
Animal ID	764	765	771	774	761	762	763	772	773	775					
Sex	M	M	M	M	M	M	M	M	M	M					
Strain	C57BL6J	C57BL6J	C57BL6J	C57BL6J	C57BL6J	C57BL6J	C57BL6J	C57BL6J	C57BL6J	C57BL6J					
Date of Surgery (8wks)	8/4/2015	8/4/2015	8/4/2015	8/4/2015	8/4/2015	8/4/2015	8/4/2015	8/4/2015	8/4/2015	8/4/2015					
Date of Sacrifice (16wks)	9/30/2015	9/30/2015	9/30/2015	9/30/2015	9/30/2015	9/30/2015	9/30/2015	9/30/2015	9/30/2015	9/30/2015					
Body weight (BW) (8wks)	20.86	19.62	20.77	21.79	20.15	23.24	21.61	22.74	24.46	21.59	20.76	22.29833333	0.1062		
Body weight (BW) (16wks)	25.35	26.83	26.94	27.44	26.5	27.69	27.14	31.6	29.88	30.25	26.64	28.84333333	0.0779		
Heart weight (HW,g)	0.1198	0.119	0.1305	0.135	0.1612	0.1611	0.1922	0.1912	0.172	0.2395	0.126075	0.1862	0.0045		
Lung weight (LW,g)	0.1724	0.1627	0.1554	0.1575	0.1458	0.163	0.1773	0.1885	0.1461	0.1818	0.162	0.1670833333	0.6197		
Tibia length (TL,m)	0.02311	0.02297	0.02301	0.02257	0.02265	0.02308	0.02299	0.02407	0.02297	0.02419	0.022915	0.023325	0.2630		
HW/BW (mg/g)	4.73	4.44	4.84	4.92	6.08	5.82	7.08	6.05	5.76	7.92	4.73	6.45	0.0050		
HW/TL (mg/mm)	5.18	5.58	5.67	5.98	7.12	6.98	8.36	7.94	7.49	9.90	5.50	7.96	0.0026		
LW/BW (mg/g)	6.80	6.06	5.77	5.74	5.50	5.89	6.53	5.97	4.89	6.01	6.09	5.80	0.4145		
LW/TL (mg/mm)	7.46	7.08	6.75	6.98	6.44	7.06	7.71	7.83	6.36	7.52	7.07	7.15	0.8140		
FS	17.923	16.767	16.231	20.934	12.238	15.521	18.979	19.796	19.071	10.416	17.96375	16.0035	0.3955		
HR	663	746	728	603	693	678	658	719	670	432	685	641.6666667	0.4865		
ENDOarea;d	4.406	4.809	4.691	6.832	6.079	6.141	6.908	7.135	5.058	8.949	5.1845	6.711666667	0.0938		
ENDOarea;s	1.357	1.367	1.222	1.901	1.97	2.057	3.52	2.201	1.519	4.035	1.46175	2.550333333	0.0694		
ENDOmajr;d	6.499	5.949	6.827	6.921	6.377	6.908	7.303	6.825	7.216	7.485	6.549	7.019	0.1173		
ENDOmajr;s	5.334	4.951	5.718	5.472	5.596	5.905	5.917	5.474	5.84	6.706	5.36875	5.906333333	0.0669		
EPIarea;d	18.949	18.053	18.333	18.991	23.983	23.925	26.02	25.657	22.804	32.292	18.5815	25.78016667	0.0033		
EPImajr;d	7.64	6.952	7.869	8.147	7.585	8.143	8.557	8.035	8.538	8.72	7.652	8.263	0.0727		
EDV	23.8526	23.8311	26.6772	39.3878	32.2919	35.3375	42.0241	40.5641	30.4033	55.7971	28.437175	39.403	0.0834		
ESV	6.029452	5.63758	5.820501	8.665093	9.183092	10.118105	17.349591	10.036212	7.38951	22.539905	6.538201	12.7694025	0.0755		
Mass (mg)	101.6188	84.7838	98.2073	94.006	125.2521	133.3493	150.6785	137.7754	138.4268	187.7776	94.659975	145.5432833	0.0025		
Vol/mass	0.234726	0.281081	0.271642	0.418992	0.257815	0.265	0.278899	0.294422	0.219634	0.297144	0.30161025	0.268819	0.3778		
SV mcl	17.82316	18.19332	20.8567	30.72271	23.10881	25.21944	24.67453	30.52787	23.01376	33.25715	21.8989725	26.63359333	0.1803		
CO mcl/m	11816.76	13572.22	15183.68	18525.79	16014.4	17098.78	16235.84	21949.54	15419.22	14367.09	14774.6125	16847.47833	0.2739		
EF	0.747	0.763	0.782	0.780	0.716	0.714	0.587	0.753	0.757	0.596	0.768	0.687	0.0733		

C57BL6J Control vs caCAMKII Data

Description / Measurement	Control				caCAMKII				
	3 NA	1	2	4	5	6	7 NA		
Used in Western Lane Number	3	1	2	4	5	6	7		
Group	Saline	Saline	cTnT-GFP	cTnT-GFP	cTnT-CAMKII	cTnT-CAMKII	cTnT-CAMKII	cTnT-CAMKII	
dose of virus (vg)			1.1E+11	1.1E+11	3.78E+11 plus GFP 1.1E+11	3.78E+11 plus GFP 1.1E+11	3.78E+11 plus GFP 1.1E+11	3.78E+11 plus GFP 1.1E+11	
Animal ID	690	695	689	694	687	688	691	692	
Sex	M	M	M	M	M	M	M	M	
Strain	C57BL6J	C57BL6J	C57BL6J	C57BL6J	C57BL6J	C57BL6J	C57BL6J	C57BL6J	
Date of Injection (3wks)	5/27/2015	5/27/2015	5/27/2015	5/27/2015	5/27/2015	5/27/2015	5/27/2015	5/27/2015	
Date of Sacrifice (6wks)	6/17/2015	6/17/2015	6/17/2015	6/17/2015	6/17/2015	6/17/2015	6/17/2015	6/17/2015	
Body weight (BW,g) (3wks)	12.89	7.71	9.9	12.14	11.09	10.47	11.29	10.95	
Body weight (BW) (6wks)	23.22	18.26	22.16	22.89	22.71	20.71	23.26	24	
Heart weight (HW,g)	0.1155	0.0945	0.1045	0.1175	0.1276	0.1533	0.1367	0.1625	
Lung weight (LW,g)	0.1498	0.1153	0.1477	0.1449	0.1462	0.1667	0.1572	0.1732	
Tibia length (TL,m)	0.02235	0.0209	0.02136	0.02126	0.02205	0.02193	0.02221	0.02239	
HW/BW (mg/g)	4.97	5.18	4.72	5.13	5.62	7.40	5.88	6.77	
HW/TL (mg/mm)	5.17	4.52	4.89	5.53	5.79	6.99	6.15	7.26	
LW/BW (mg/g)	6.45	6.31	6.67	6.33	6.44	8.05	6.76	7.22	
LW/TL (mg/mm)	6.70	5.52	6.91	6.82	6.63	7.60	7.08	7.74	
FS	17.265	12.435	12.59	18.161	16.706	7.563	14.999	19.315	
HR	591	707	604	407	708	597	458	652	
ENDOarea;d	8.321	6.836	9.693	10.211	8.507	18.843	11.191	15.131	
ENDOarea;s	3.326	2.16	4.415	2.891	4.918	16.592	5.711	11.277	
ENDOmajr;d	6.81	6.572	6.375	7.325	6.43	8.208	7.555	7.904	
ENDOmajr;s	5.634	5.755	5.573	5.995	5.356	7.587	6.422	6.377	
EPIarea;d	19.596	17.458	19.631	21.509	22.917	32.869	21.421	30.067	
EPImajr;d	7.614	7.422	7.289	8.19	7.435	9.064	8.403	8.848	
EDV	47.203	37.424	51.473	62.305	45.565	128.835	70.428	99.623	
ESV	15.609	10.355	20.496	14.437	21.942	104.861	30.551	59.904	
Mass(mg)	80.971	74.066	71.135	88.693	101.227	125.354	83.521	128.133	
Vol/mass	0.583	0.505	0.724	0.702	0.450	1.028	0.843	0.777	
SV mcl	31.593	27.069	30.978	47.868	23.623	23.974	39.877	39.719	
CO mcl/m	18671.74	19137.54	18710.51	19482.09	16725.24	14312.24	18263.82	25896.85	
EF	0.669	0.723	0.602	0.768	0.518	0.186	0.566	0.399	

Avg-Ctl	Avg-caCAMII	p value (ttest)
10.66	10.856	0.857
21.6325	22.416	0.540
0.108	0.13962	0.019
0.139425	0.16056	0.047
0.0214675	0.02212	0.058
5.00	6.24	0.023
5.03	6.31	0.024
6.44	7.18	0.056
6.49	7.26	0.072
15.113	14.678	0.871
577.250	615.000	0.623
8.765	12.655	0.130
3.198	8.863	0.064
6.771	7.406	0.163
5.739	6.330	0.208
19.549	25.823	0.058
7.629	8.330	0.109
49.601	79.985	0.133
15.224	49.175	0.094
78.716	106.192	0.036
0.629	0.739	0.393
34.377	30.810	0.561
19000.47	18584.51	0.857
0.691	0.431	0.016



**Table S5. Summary statistics for cardiomyocyte-specific Sorbs2 knockout mice.**  
**Table supplements data plotted in Figure 4. Mean values were binned on weeks on age for WT and Sorbs2-cKO mice. P-values indicate difference between WT and cKO curves analyzed using 2-way ANOVA with Sidak's multiple comparisons testing the interaction between age and genotype.**

### Ejection Fraction

Bin (weeks)	WT (mean)	cKO (mean)	(pval)
10-20	0.793	0.765	0.362
20-30	0.883	0.847	0.067
30-40	0.798	0.687	0.035
40-50	0.832	0.596	9.48E-09
50-60	0.840	0.419	7.23E-21

### Indexed EDV

Bin (weeks)	WT (mean)	cKO (mean)	(pval)
10-20	0.365	0.377	0.735
20-30	0.374	0.418	0.301
30-40	0.422	0.483	0.120
40-50	0.369	0.495	3.07E-04
50-60	0.389	0.734	9.54E-11

### LV Mass

Bin (weeks)	WT (mean)	cKO (mean)	(pval)
10-20	60.067	59.129	0.826
20-30	71.044	69.945	0.795
30-40	95.392	96.634	0.763
40-50	82.019	85.332	0.421
50-60	78.739	95.106	0.001

### LV Thickness

Bin (weeks)	WT (mean)	cKO (mean)	(pval)
10-20	0.756	0.760	0.911
20-30	0.772	0.746	0.638
30-40	0.841	0.794	0.131
40-50	0.832	0.862	0.238
50-60	0.841	0.777	0.018

### Atria / BW

Bin (weeks)	WT (mean)	cKO (mean)	(pval)
10-20	0.270	0.397	0.094
20-30	0.328	0.427	0.138
30-40	0.218	0.335	1.03E-04
40-50	0.256	0.496	4.29E-05
50-60	0.208	0.982	1.87E-08
60-70	0.319	1.058	0.022

### Ventricle / BW

Bin (weeks)	WT (mean)	cKO (mean)	(pval)
10-20	3.758	3.965	0.560
20-30	3.654	3.955	0.448
30-40	3.354	3.164	0.219
40-50	3.372	3.502	0.515
50-60	3.377	4.298	1.74E-05
60-70	3.252	3.623	0.377

## Supplemental Figure Legends:

### Figure S1. Transcriptional dysregulation of Sorbs2 in heart failure.

(A-C) Human Sorbs2 transcript expression analysis of RNA sequencing data acquired from SRA archive PRJNA477855 remapped using the Kallisto/Sleuth pipeline. Sorbs2 transcript numbers are listed on X-axis in panel C. Black bars are high-confidence protein-coding transcripts with complete CDS, grey bars are transcripts with incomplete CDS, white bars are non-coding transcripts. Sample sizes are N=14 (Nonfailing), N=13 (Ischemic Cardiomyopathy, ISCH), N=37 (Dilated Cardiomyopathy, DCM), \*  $p < 0.05$ , compared to nonfailing. (A) Differential expression (Log<sub>2</sub>-fold-change) of transcripts in dilated cardiomyopathy. (B) Differential expression of Sorbs2 transcripts in Ischemic cardiomyopathy. (C) Average expression of Sorbs2 transcripts in non-failing hearts, sorted from most to least abundant with a lower cutoff of TPM>1, (represents 18 of 65 transcripts). (D) Left axis, RNA and ribosome reads, and on right axis translational efficiency (TE) plotted from public ribosomal profiling data in nonfailing and DCM human hearts from Van Heesch, et. al.<sup>17</sup> Both RNA and Ribosome reads are significantly upregulated in DCM hearts, suggesting that cardiac Sorbs2 expression at baseline and disease is primarily under transcriptional rather than translational regulation (i.e., TE = 1 and is not significantly different in DCM).

### Figure S2. Sorbs2 genetic loci in human and mice

(A) Sorbs2 genetic locus in humans. Vertical pink lines denote exon junctions. Green boxes denote the location of annotated protein domains, as well as the location of a cardiac-specific exon. Black boxes denote the alignment of three different SORBS2 clones published related to cardiac research. Blue (Ribosome) and Red (RNA) tracks show sequencing data from human hearts (adapted from Van Heesch, et.al<sup>17</sup>). Protein coding transcript tracks list those with complete CDS annotations (Gencode Basic, 8 of 65 putative transcripts). To the right is transcript abundance in nonfailing human hearts based on RNA sequencing data described in [Figure S1C](#). Abbreviations SoHo = Sorbin Homology Domain, SH3 = SRC Homology 3 Domain, ZnF-C2H2 = C2H2-type Zinc Finger (RNA-binding domain). Note this RNA-binding domain is encoded by Addgene plasmid #74514, which was used to show Sorbs2-RNA binding activity of cardiac ion channels<sup>29</sup>, however it is located in an exon that is not expressed in human heart tissue, or present in two clones obtained from heart cDNA, including “our clone”, which was obtained by RT-PCR amplification of the cardiac-specific Sorbs2 isoform from mouse heart cDNA. (B) Sorbs2 genetic locus in mice, with a similar track layout. Note the red box indicating the obligate exon 12 with flanking loxP sites. These mice were crossed to  $\alpha$ MHC-CRE expressing line to generate cardiomyocyte-specific Sorbs2 knockout mice (Sorbs2-cKO). The two tracks of black peaks represent Ribosome and RNA sequencing data specifically from cardiomyocytes, remapped from SRA-PRJNA484227<sup>19</sup>. Bar graph on right shows TPM expression of Sorbs2 protein coding transcripts (Gencode Basic, 11 of 37 putative transcripts) in mouse hearts from RNAseq data. ZnF-C2H2 represents the location of the defined RNA-binding domain in transcripts that are not abundant in hearts or cardiomyocytes. The cardiac-specific Sorbs2 exon remains unannotated in mouse reference transcriptomes yet is clearly present in RNA and Ribosome sequencing data.

### Figure S3. Cardiomyocyte-specific Sorbs2 knockout mice.

(A) Western blot showing expression of Sorbs2, in WT and cKO heart samples from female mice at ~12 months age using an independent antibody (Sigma mouse monoclonal). Also shown on left side is a positive control (Sorbs2 plasmid cloned from mouse heart cDNA expressed in HT1080 cells), as a confirmation of on-target antibody binding. (B) Western blot of Sorbs1 expression from WT and cKO heart tissues does not show compensatory changes in Sorbs1 expression following cardiomyocyte loss of Sorbs2. Gapdh shown as loading control for panels A and B. (C) Representative Sorbs2 immunofluorescence (green) in heart sections from wildtype (WT) mice, co-localized with N-Cadherin (CDH2, red) at the intercalated disc (ICD). Also note Sorbs2 reactivity in the coronary artery on the right picture.

### Figure S4. Cardiomyocyte-specific Sorbs2 knockout mice develop age-related systolic dysfunction, cardiac remodeling, and premature death.

(A) Representative serial m-mode echocardiographic images from one WT and one Sorbs2-cKO mice. The callout indicates the ejection fraction (EF) for that mouse calculated using the Endocardial and Epicardial traces (see Methods section 2.3). At three months old (first row) both WT and cKO mice show normal wall motion, wall thickness, and chamber dimensions in systole and diastole. At 10 months (second row) Sorbs2-cKO heart shows reduced wall motion, increased chamber dimension, and decreased EF. At 12 months old, (third row) Sorbs2-cKO hearts show significant LV systolic dysfunction with a big chamber, thin walls, and poor wall motion. (B) Time course of echocardiography from WT and Sorbs2-cKO hearts indicates trending to increased RV thickness in cKO hearts, coincident with emerging HF. (C) Postmortem gravimetric analyses of heart chamber mass in ~48-week male mice, normalized to bodyweight (BW). The left atrium (LA) is significantly enlarged in Sorbs2-cKO hearts compared to control, whereas, the right atrium (RA), the left ventricle plus septum (LV+S) and the right ventricle (RV) are not different. Dots show individual hearts, N=6 per group, with mean +/- SEM. Significance from t-test, \* p<0.05, ns = not significant. (D) Postmortem gravimetric analysis of atrial mass normalized to either body weight (BW) or ventricular mass in mice 12-24 weeks of age. Dots show individual hearts with mean +/- SEM. Significance from t-test, \* p<0.05, \*\*p<0.01. (E) Male ratio of postmortem LA/RA mass over time (cKO regression,  $r^2=0.596$ ,  $p=2e^{-4}$ ). This indicates increases in LA mass rather than RA or bi-atrial mass are driving the significant increase in total atrial mass shown in [Figure 3D](#). (F) Male correlation of atrial to ventricle size in WT and cKO mice hearts (cKO regression,  $r^2=0.479$ ,  $p<1e^{-4}$ ).

### Figure S5. Cardiomyocyte-specific Sorbs2 knockout mice have severe contractile dysfunction.

(A) Datapoints represent the group mean +/- SEM change in heart rate from baseline through increasing dobutamine (DOB) concentrations (N=7 mice per group), and a black trendline denotes a linear regression fit from baseline through the highest dose (12 ng/g/min). No difference was found. These data show that Sorbs2-cKO hearts are unable to increase cardiac contractility in response to DOB despite having equivalent increases in heart rate. (B) Final 30 second average per dose for dP/dT Min. Dots show individual mice with mean +/- SEM,

statistics acquired using one-way ANOVA with Sidak posthoc test comparing selected groups (each comparison shown on plot), \*  $p < 0.05$ , ns = not significant. (C-F) Waterfall plots of EKG intervals (30 seconds stacked back to front) in WT and Sorbs2-cKO mice. (C) WT hearts have normal sinus rhythm with regular R-R, P-P, and P-R intervals. (D) cKO hearts also show normal sinus rhythm and intervals, despite obvious bifid P-waves, increased P duration, and QRS duration. (E-F) WT and cKO hearts after DOB challenge, both have expected increase in heart rate, indicated by reduced R-R interval, and maintain sinus rhythm.

**Figure S6. Cardiomyocyte-specific Sorbs2 knockout mice have dysregulated cytoskeletal protein expression not ICD.**

(A-D) Heatmaps reprint from [Figure 6](#) alongside digitized western blot images that show analysis of protein expression from WT and Sorbs2-cKO cardiac lysates at 3, 6, and 12 months of age. Each box represents the mean integrated intensity, normalized to loading control and expressed relative to 3-month WT;  $n=4$  mice per group. Significant differences ( $p < 0.05$ ) denoted with (\*, black for down-regulated and white for up-regulated) overlay on the heatmap, were acquired using t-test comparing cKO to WT at each age. (Abbreviations: CS = Cell Signaling, AB = Abclonal). Heatmaps and blots are organized by (A) intercalated disc (ICD) proteins, (B) ion channels and calcium handling proteins, (C) sarcomere proteins, and (D) structural cytoskeletal proteins.

**Figure S7. Cardiomyocyte-specific Sorbs2 knockout mice have normal localization of cytoskeletal and ICD proteins.**

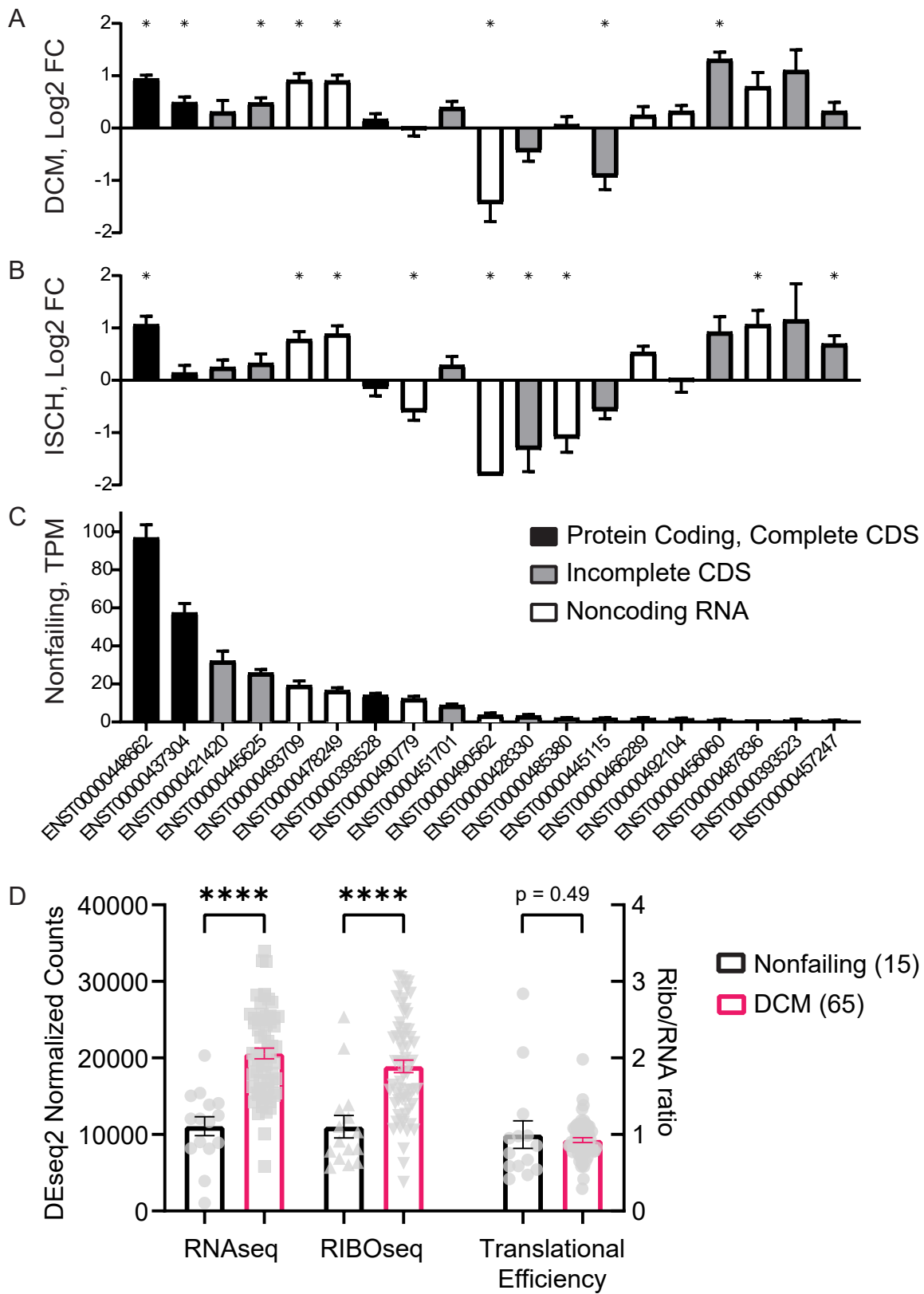
(A-B) Representative immunofluorescent microscope images of heart tissue oriented with longitudinal myofibers from (A) WT and (B) Sorbs2-cKO mice. Inset pictures show staining with (1) wheat germ agglutinin (WGA) in green, (2) Sorbs2 in white, (3) Ctnnb1 in red, and (4) a color overlay. A blinded review of images from WT and cKO mice for Ctnnb1 localization and several other cytoskeletal and ICD proteins (C-F) were indistinguishable from each other, ( $n=4$  images per mouse and  $n=4$  mice per group). These include (C) phalloidin staining actin fibers in red, (D) alpha actinin 2 (Actn2) staining Z-disk and sarcomeres in red, (E) vinculin (Vcl) staining ICDs and costameres in white, and (F) connexin 43 (Gja1) staining ICDs and vasculature in white. Representative WT images shown on the top row with cKO images on the bottom row.

**Figure S8. Sorbs2 regulation of intracellular calcium and Scn5a activity *in vitro*.**

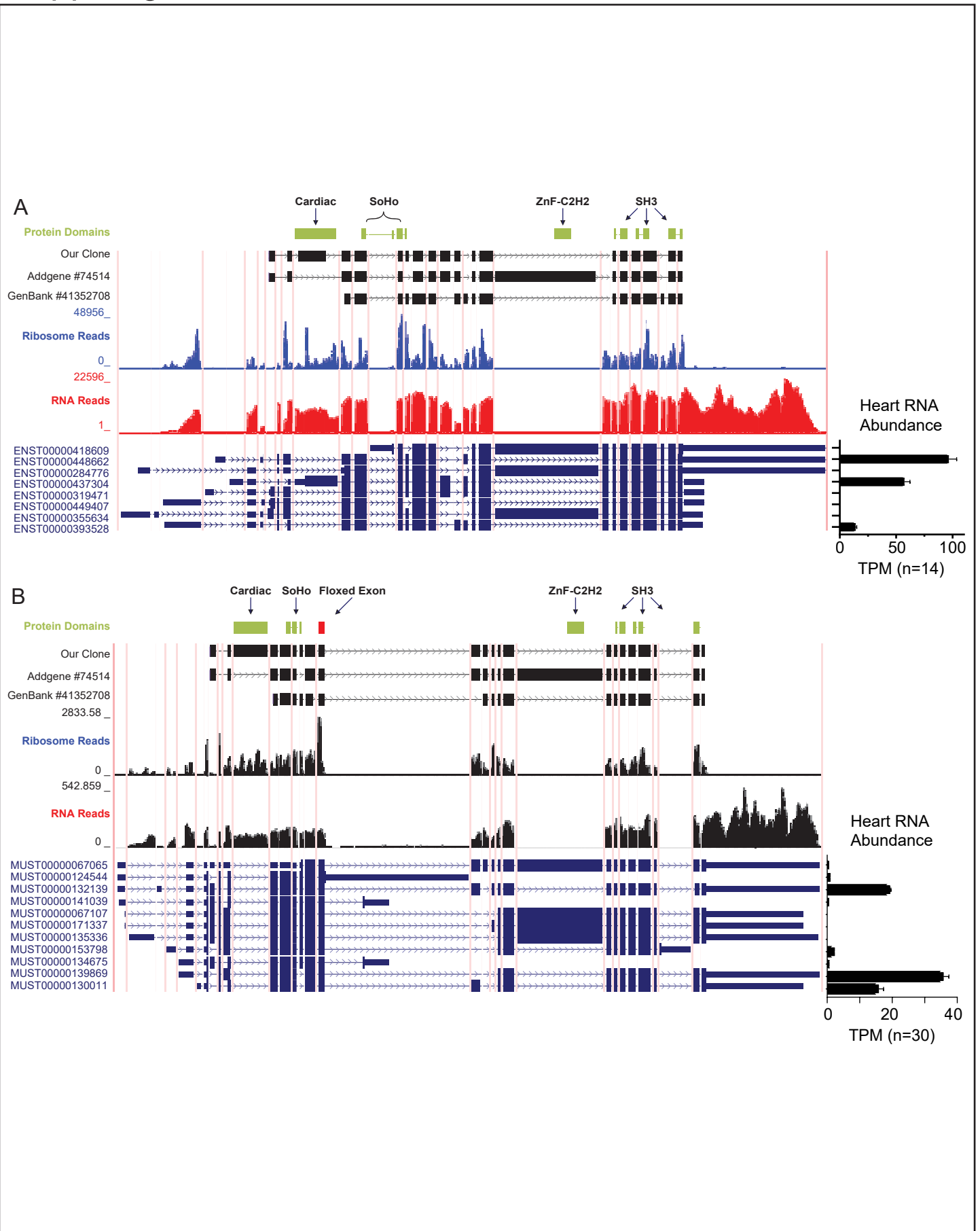
(A) Western blot analysis of Sorbs2 protein levels in NRCMs transiently transfected with control or Sorbs2 siRNAs for ~48 hours. TUBB shows consistent loading. (B) Intracellular calcium signal intensity from Fura-2AM loaded NRCMs. Data were acquired in 4 independent experiments, 2 plates per experiment per condition with ~40-50 cells analyzed per plate. Dots represent individual cells with mean  $\pm$  SEM, statistics are acquired from T-test, \*\*\*\*  $p < 0.0001$ , ns=not significant. (C-D) Overexpression or knock down of Sorbs2 did not significantly alter sodium current-voltage relationships derived from electrophysiology experiments in transiently transfected NRCMs. (E-F) Peak current density is also not significantly different. Data shown are mean SEM, with individual cells plotted in (D, E),  $N = 5-7$  cells per treatment, statistics are acquired from T-test, ns = not significant.



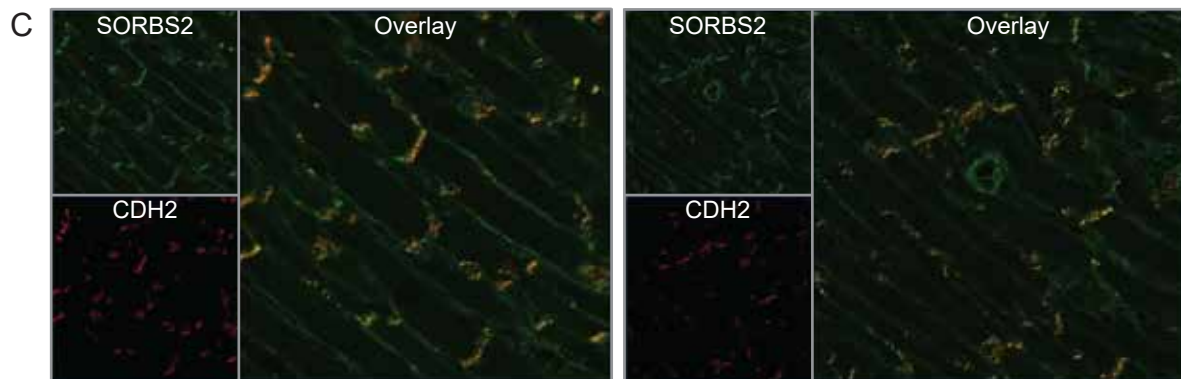
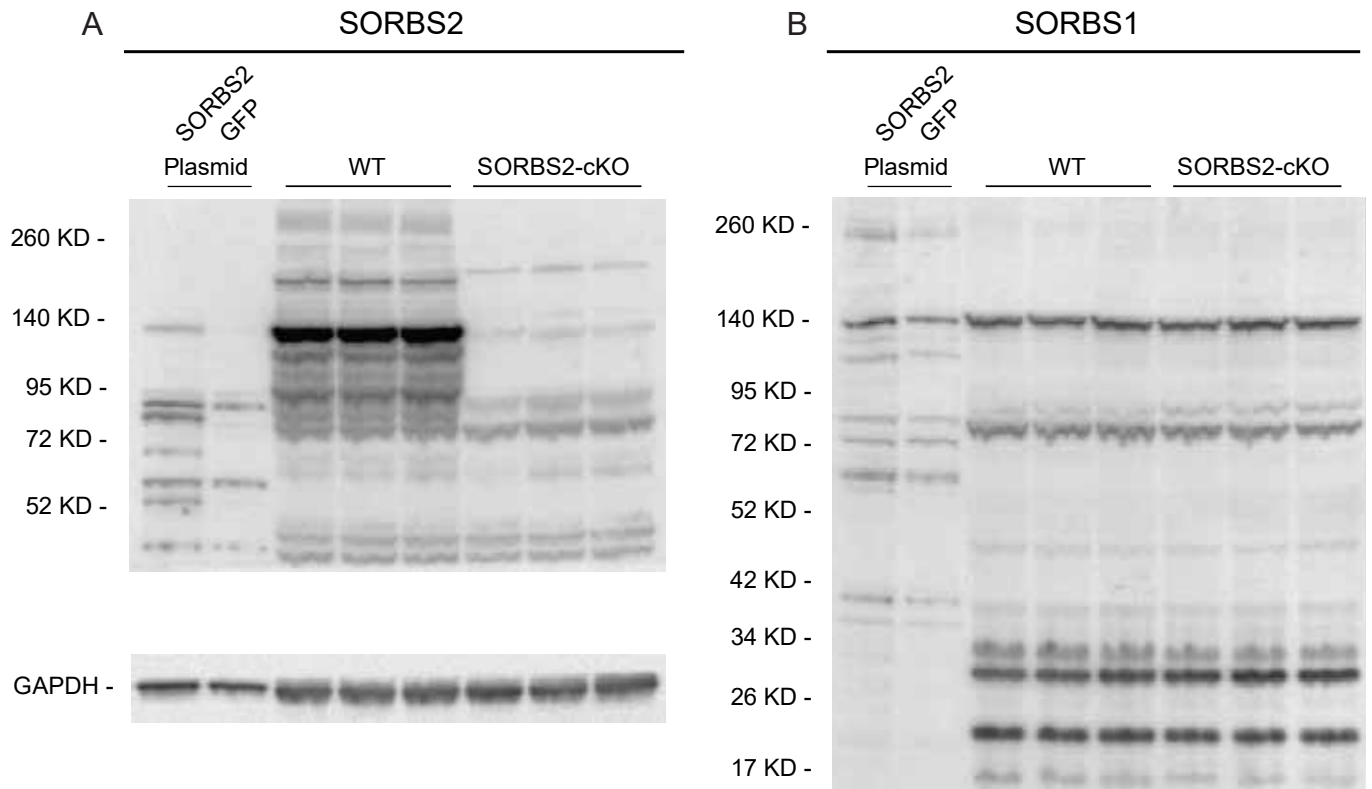
# Supp. Figure 1



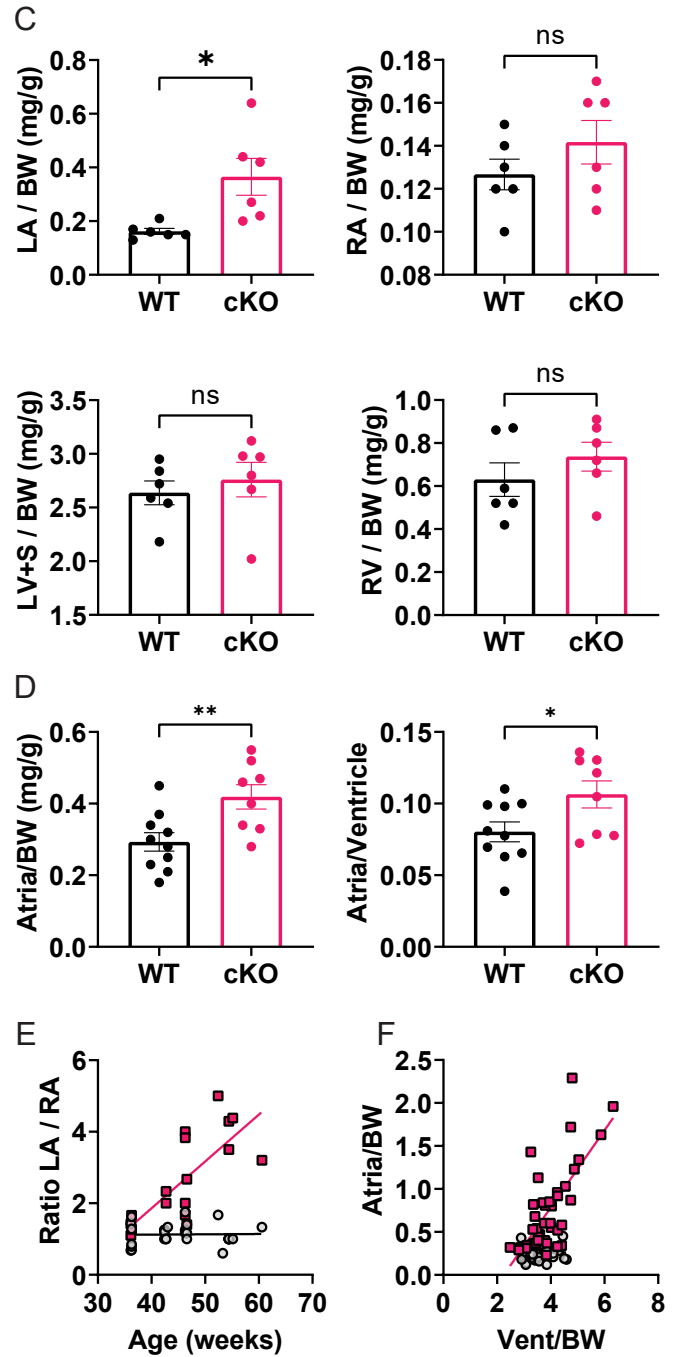
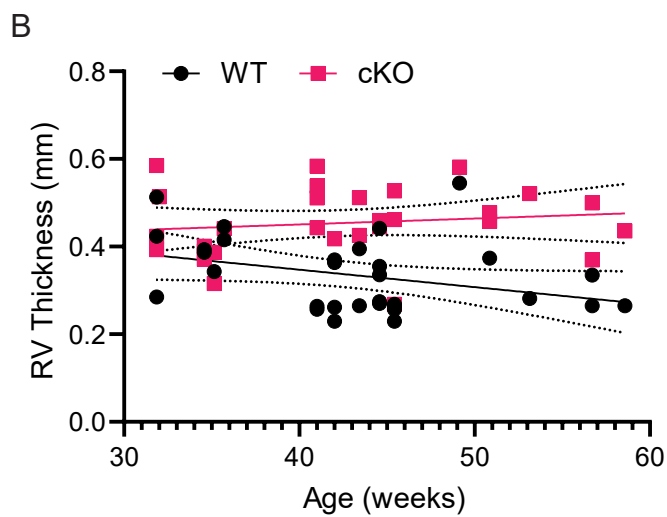
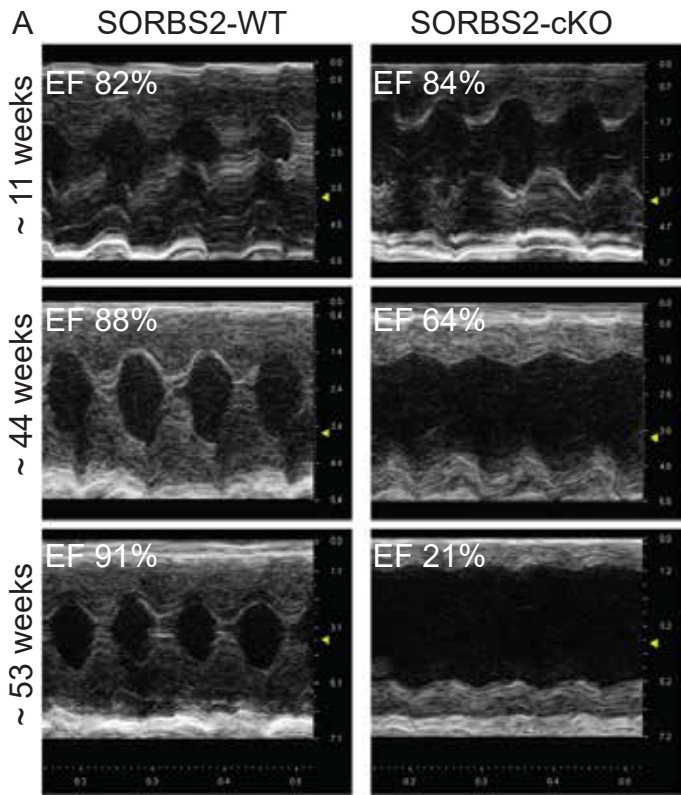
# Supp. Figure 2



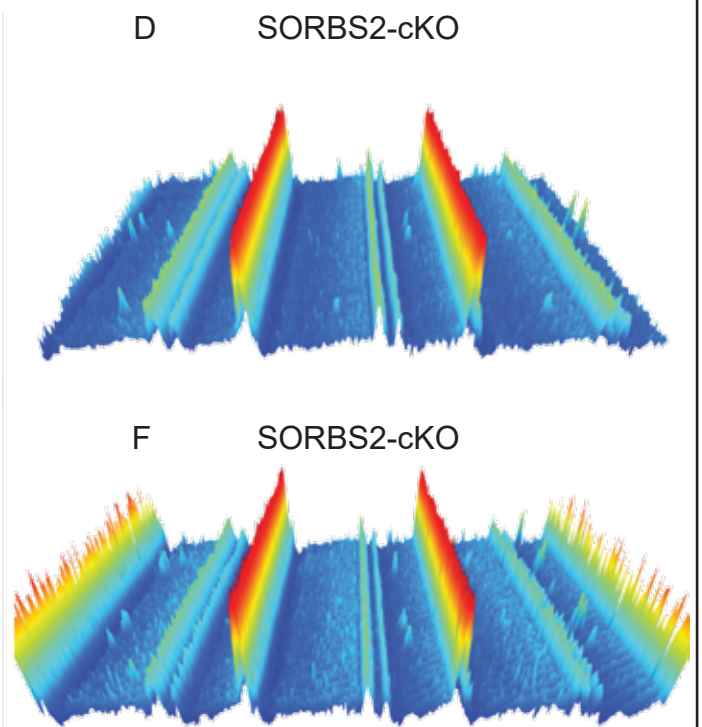
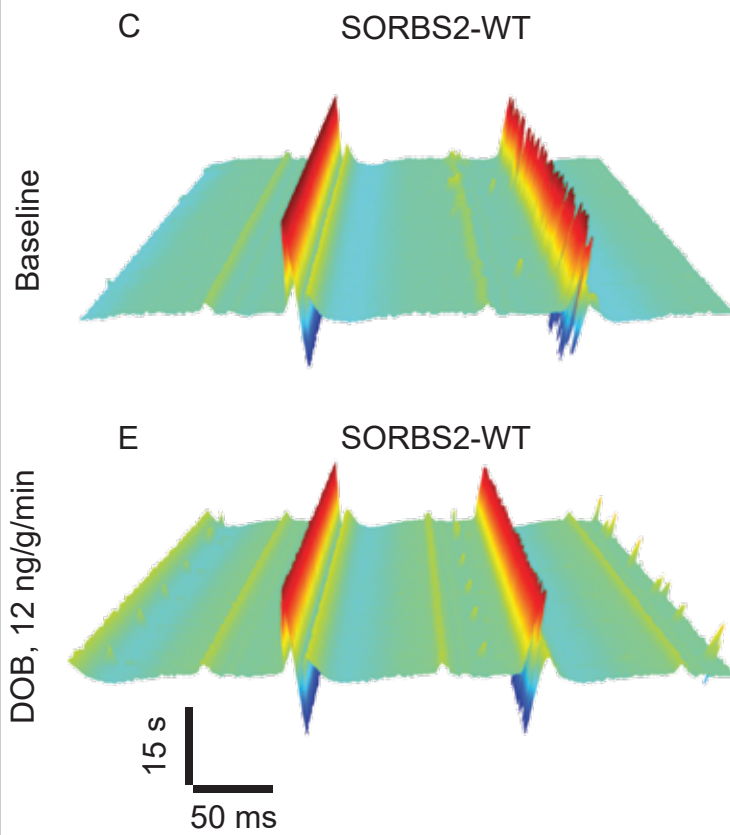
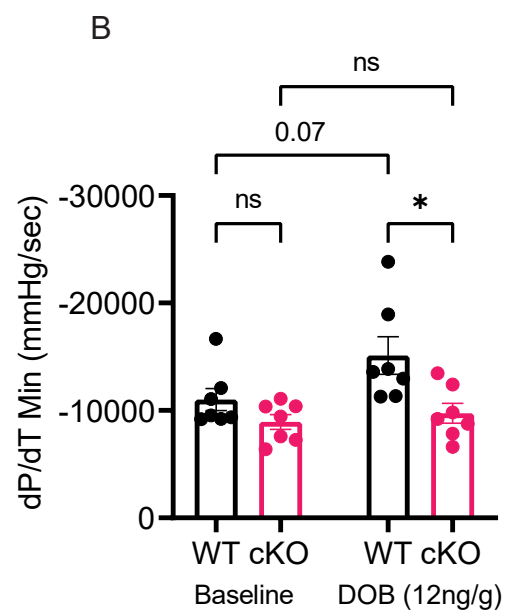
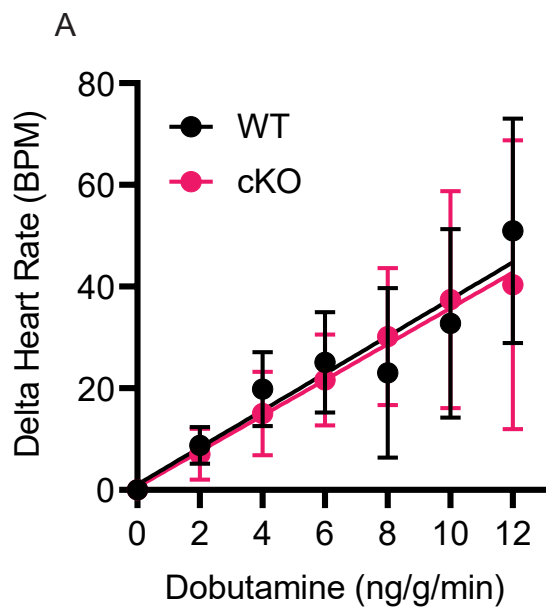
# Supp. Figure 3



# Supp. Figure 4

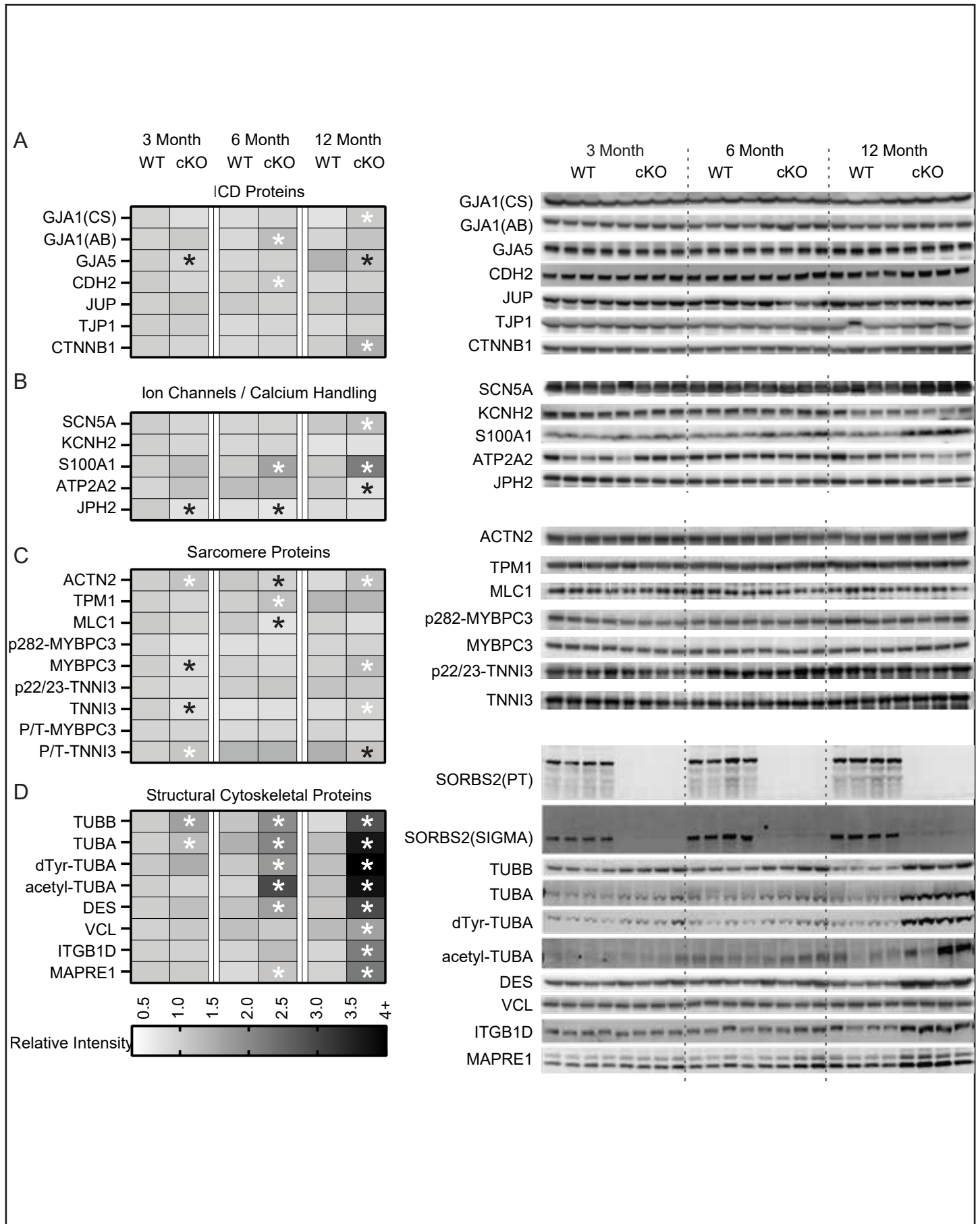


# Supp. Figure 5

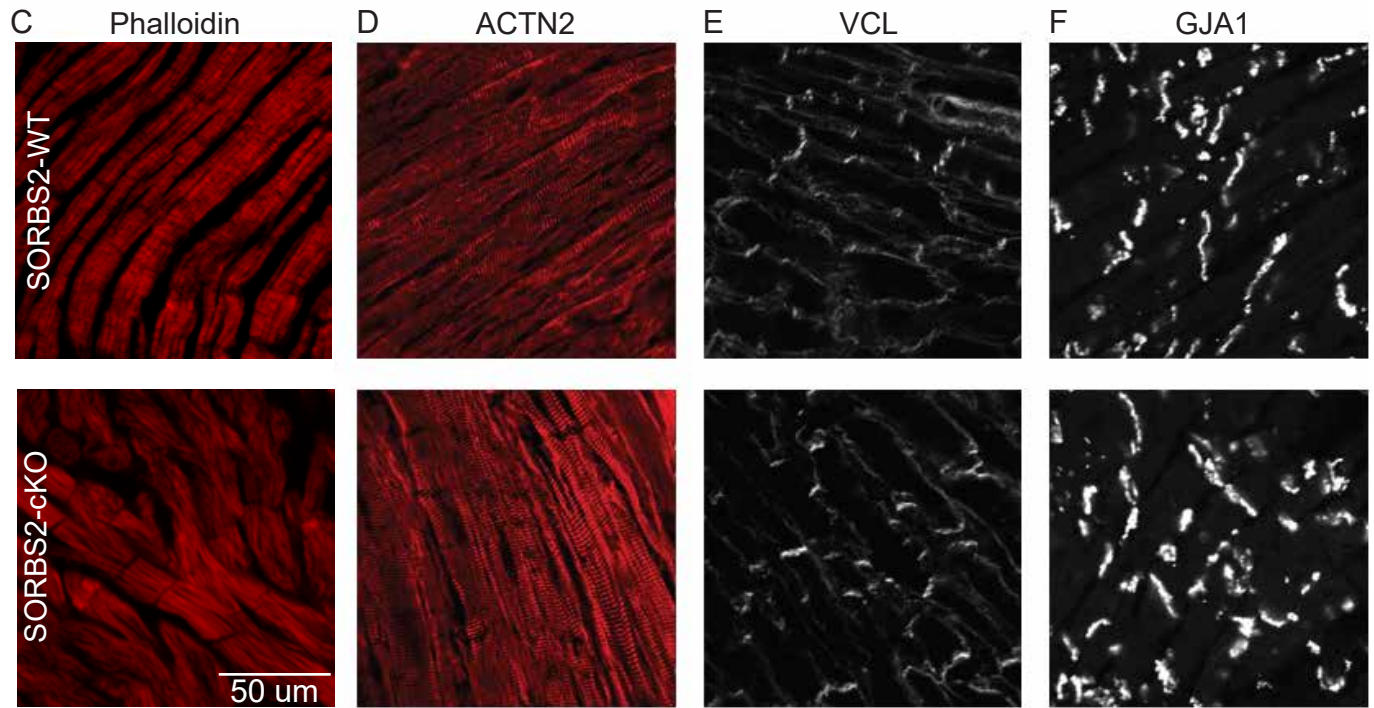
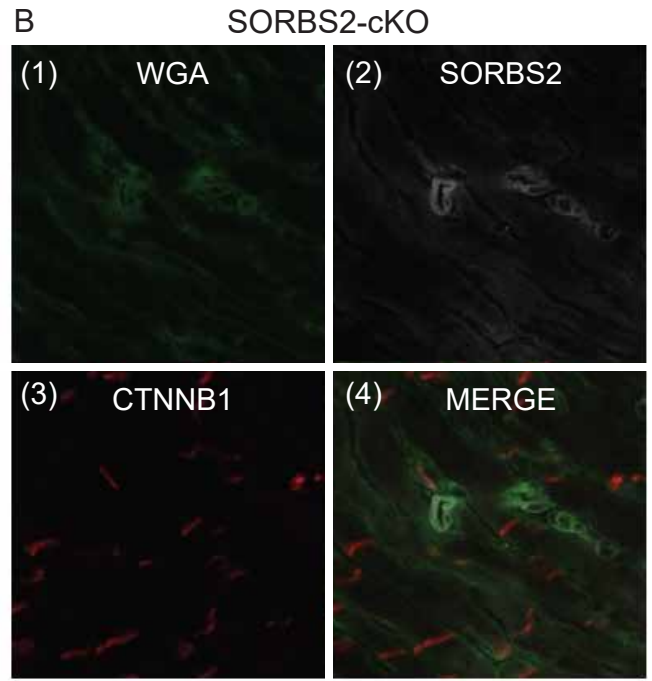
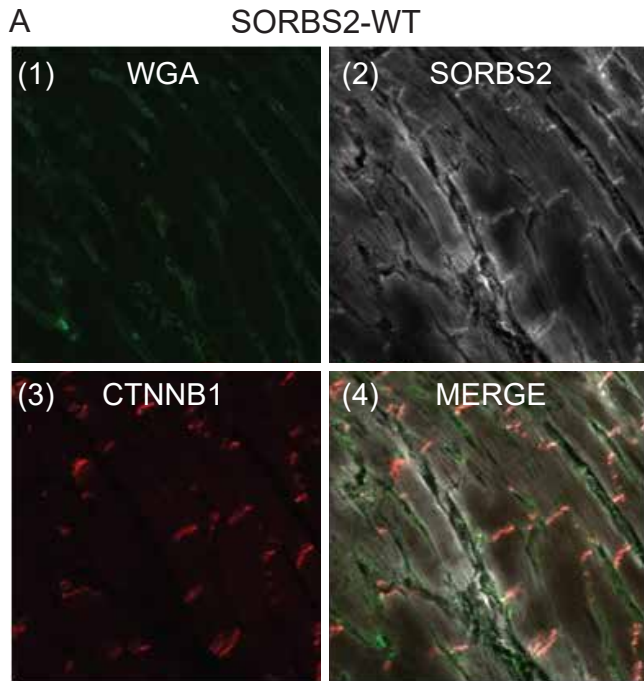




# Supp. Figure 6



# Supp. Figure 7



# Supp. Figure 8

